UNIVERSITY OF JYVÄSKYLÄ

MASTER'S THESIS

DEPARTMENT OF PHYSICS

Analysis of linear alkylbenzene samples with a camera-based equipment

Author
Heidi Rytkönen

Supervisors
Jari Joutsenvaara
University of Oulu
Kai Loo
University of Jyväskylä

December 12, 2017

Abstract

Rytkönen, Heidi
Analysis of linear alkylbenzene samples with camera based equipment
Master's thesis
Department of Physics, University of Jyväskylä, 2017, 67 pages.

Use of liquid scintillator detectors has been an increasing trend in neutrino physics within the last decades. The light yield of scintillator detectors surpasses the traditional Cherenkov counters and availability of low-cost and relatively safe compounds (linear alkylbenzenes) as liquid scintillator solvent allows the construction of larger neutrino detectors. A downside of liquid scintillators is their tendency to get easily contaminated and undergo changes via exposure to UV light and elevated temperatures. For these reasons, purification and optical properties of liquid scintillators must be studied to make them suitable for large neutrino detectors.

In this study a set of linear alkylbenzene samples were purified by a standard method used in chemistry called column chromatography: the samples were passed through a fine purification material (aluminum oxide, Al_2O_3) several times. The transparency measurements for the samples were carried out via a setup using a Raspberry camera module as a light detector. The long attenuation length of linear alkylbenzene is problematic for light measurements since it means that the setup must be long enough to detect differences between the purified samples. This setup was built to examine if it is possible to detect differences with this kind of low-cost setup.

Results showed that the current setup is not precise enough to detect any differences between samples with long attenuation lengths. The setup is ideally able to distinguish samples that have at least difference of 0.4 % in their absorbance. The path length of LAB (50 mm) was not long enough to decrease the light input so that the samples would have had differences over 0.4 %.

Keywords: linear alkylbenzene, liquid scintillator counting, C14 experiment, Callio Lab

Tiivistelmä

Rytkönen, Heidi
Bentseenin alkyylijohdannaisten analyysi kameran käyttöön pohjautuvalla laitteistolla
Pro Gradu -tutkielma
Fysiikan laitos, Jyväskylän yliopisto, 2017, 67 sivua.

Nestemäisiä tuikeaineita hyödyntävät ilmaisimet ovat saaneet jalansijaa neutriinofysiikassa viime vuosikymmeninä. Perinteisiin Cherenkovin ilmaisimiin niiden etu on suurempi hiukkasten vuorovaikutuksesta aiheutuvan valon tuotto. Lisäksi edullisten, suhteellisen ympäristöystävällisten ja optisesti kirkkaiden tuikeaineyhdisteiden (bentseenin alkyylijohdannaiset) saatavuus mahdollistaa yhä suurempien ilmaisimien rakennuksen. Nestemäisten tuikeaineiden ongelmana on kuitenkin niiden taipumus kerätä epäpuhtauksia itseensä ja niiden muutosalttius UV-säteilyn ja korkeiden lämpötilojen vaikutuksesta. Muutokset heikentävät tuikeaineiden valon tuottoa, ja siksi nestemäisten tuikeaineiden puhdistusta ja optisia ominaisuuksia on tutkittava, jotta saatavilla on mahdollisimman tehokas kohtio neutriinoille.

Tässä tutkimuksessa erä bentseeninäytteitä puhdistettiin kemiassa yleisesti käytössä olevalla menetelmällä, pylväskromatografialla: näytteet suodatettiin hienojakoisen alumiinioksidin (Al_2O_3) läpi useaan kertaan. Näytteiden kirkkautta mitattiin laitteistolla, jossa Raspberry Pi -minitietokoneen kameramoduulia käytettiin valosensorina. Bentseenin alkyylijohdannaisten pitkä vaimenemispituus aiheuttaa ongelmia mitattaessa valon vaimenemista: laitteiston tulisi olla niin pitkä, että näytteiden erot kirkkaudessa saataisiin erotettua paremmin. Tutkimuksen tarkoituksena on myös selvittää onko eroja mahdollista havaita pienemmällä ja edullisemmalla laitteistolla.

Tuloksien mukaan laitteisto ei pysty nykyisessä muodossaan erottamaan näytteitä, joilla on hyvin pitkä vaimenemispituus. Ihanteellisessa tilanteessa laitteistolla on mahdollista havaita eroja näytteiden välillä, joiden absorptiossa on $0,4$ % ero. Näytesäiliöiden pituus (50 mm) ei ollut tarpeeksi suuri, jotta valo olisi vaimentunut tarpeeksi.

Avainsanat: bentseenin alkyylijohdannaiset, nestemäiset tuikeaineet, C14 koe, Callio Lab

Contents

1 Introduction

Devices utilizing scintillators, materials that convert incident radiation to light, have had a role in particle detection since almost as early as the discovery of radioactivity. The earliest usage of scintillators in particle detection is from 1903. An instrument consisting ZnS screen as a scintillator was developed by Crookes and was used to visually observe the light flashes caused by alpha particles. It was not a very popular way for particle detection for the fact that it was tedious to use. In 1944 by Curran and Baker added photomultiplier tubes (PMTs) to collect the scintillation light. Scintillations could be counted more efficiently which led to a rapid development of scintillation counters. [1]

Today scintillation counting is a widely used technique in many fields. Security sector and medicine, for example, need X-ray machines to identify objects and materials and some of them take advantage of scintillation counters. The fact that they are fast instruments and they offer a high counting efficiency makes them great devices for many research topics such as lifetime measurements on unstable particles or study of cosmic rays. Even after 70 years on the development of the modern scintillation counter, there is still much effort put into investigating the technology: improving the sensitivity of the detectors enables us to study low energy processes and these studies may result in discoveries beyond the standard model in particle physics.

1.1 Background

Experimental research of neutrinos, fermionic elementary particles, relies heavily on large neutrino detectors. Neutrinos cannot be detected directly since they do not carry an electric charge and thus do not ionize matter. For this reason, the detection of neutrinos can be done for example via a process called inverse beta decay [2]

$$\bar{\nu}_e + \mathrm{p} \;\rightarrow\; \mathrm{e}^+ + \mathrm{n}, \tag{1}$$

where the energy of antineutrinos can be derived from the measured positron kinetic energy $\mathrm{E}_{\bar{\nu}_e} \approx \mathrm{E}_{\mathrm{e}^+} + \mathrm{E}_{\mathrm{thr}} = \mathrm{E}_{\mathrm{e}^+} + 1.8$ MeV. Because the cross-section of this event is approximately $0.0952 \left(E_e^{(0)} p_e^{(0)} / 1 \text{ MeV} \right) \times 10^{-42}$ cm^2 [3] its probability to occur is very low. Therefore to detect a meaningful number of neutrinos the detector must be very large.

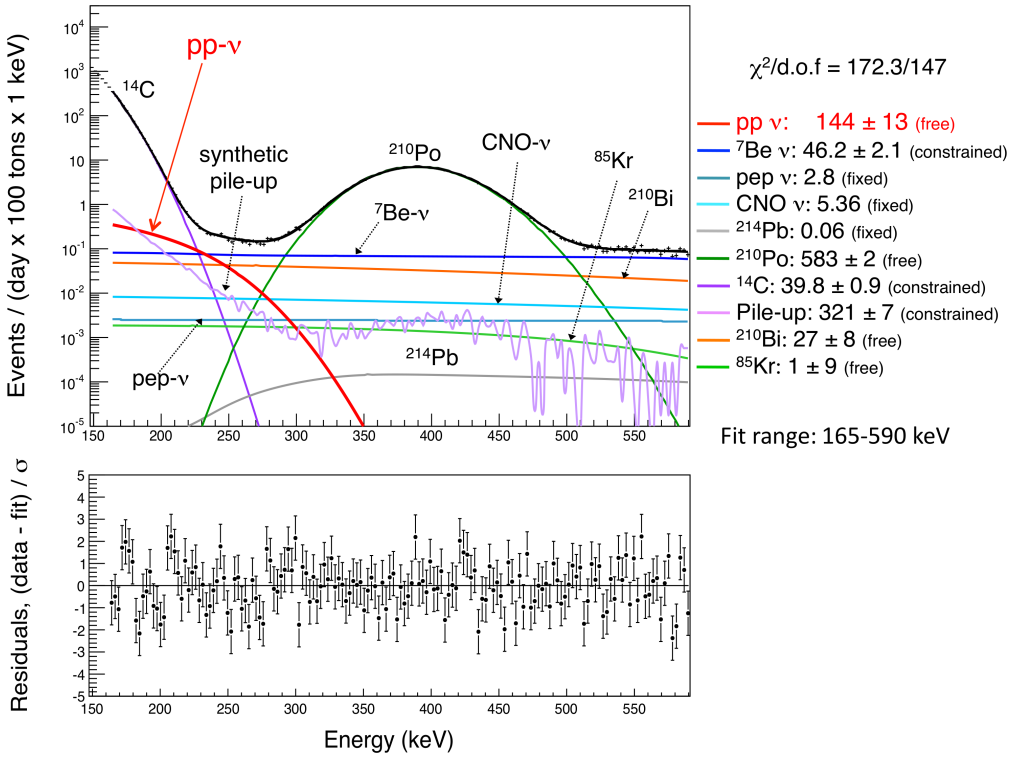

Figure 1: Energy spectrum of Borexino from 165 keV to 590 keV. Evidently, ^{14}C decays contribute the most at the low energies. The spectrum of low-energy solar neutrinos from proton-proton reaction is the red curve (pp-ν). Figure from [5].

Many existing neutrino detectors are so-called Cherenkov detectors. Neutrinos are detected via neutrino-electron elastic scattering in which energy from a neutrino is transferred to an electron. The recoil energy causes the electron to travel through the detector medium faster than the speed of light in that medium. Consequently, the electron emits Cherenkov light in a cone around the direction of the motion. This enables the determination of the direction of the electron, and furthermore, the direction of the neutrino. The medium used in Cherenkov detectors is water and though water is safe to use, available in large volumes at low cost, and easy to purify, detectors based on liquid scintillators are also becoming more common in neutrino studies. In Cherenkov detection, there is a minimum neutrino energy which can be detected due to the fact that the electron needs a certain amount of energy to emit Cherenkov light. Liquid scintillation counters, on the contrary, can be used to detect low-energy neutrinos. Moreover, liquid scintillator can produce roughly 30 times more light than water. [4, 2]

Linear alkylbenzenes (LAB) are prominent chemical compounds found to be suitable for large liquid scintillator detectors used in neutrino experiments. Such experiments are SNO+ in SNOLAB (Sudbury, Ontario in Canada) [6] and JUNO, an experiment under construction at Kaiping, Jiangmen in China [7]. SNO+ is a successor to SNO experiment, another neutrino experiment using heavy water instead of liquid scintillator, and its primary goal is to detect neutrinoless double beta decay. JUNO on the other hand will focus on determining neutrino mass hierarchy and mixing angles with a higher precision than before. When the constructions are finished JUNO will be the largest liquid scintillator counter ever build with a 34.5 m diameter acrylic sphere containing 20 kt linear alkylbenzene [7].

Linear alkylbenzene is also a subject of research in C14 experiment [8] that is an ongoing experiment in Callio Lab (Lab 2), Pyhäsalmi Mine [9]. The purpose of C14 experiment is to find a LAB sample with a $^{14}C/^{12}C$ ratio smaller than 10^{-18}. A typical biological organism such as a human being has an isotopic ratio $^{14}C/^{12}C$ of 10^{-12} [10]. This means that the aim is to find material that has one million times less radioactive carbon than in living organisms which makes it a challenging task. The radioactive isotope of carbon ^{14}C (decays via β^- decay with half-life of $t_{1/2} = 5,730$ years and maximum energy of Q= 156 keV [10]) is produced naturally by the neutron reactions caused by cosmic rays in the atmosphere and by the decays of radioactive elements (uranium and thorium) in the bedrock. In organic liquid scintillators radiocarbon causes unavoidable background for the measurements of low-energy neutrinos. Such neutrinos are for example the low energy neutrinos coming from the Sun. Figure 1 shows the radiocarbon spectrum in case of the solar neutrino experiment Borexino [5].

1.2 Motivation

A problem concerning LAB samples is that their purity varies from sample to sample. The impurities in LAB belong to many different chemical groups: fluorene, naphthalene derivatives, biphenyl derivatives, diphenyl alkane, and small amounts of alcohol, ketone, and ester [7]. These impurities cause inconsistencies in measurements and decrease the effectiveness of detector. Because of the impurities LAB must be purified properly and its optical properties must be studied.

Devices used to determine the optical transparency of liquid scintillators can be rather expensive. Precise transparency meters require hardware having at least price of four to five digit number. Fast measurements that give directional

results can be made with a much simpler and less expensive method. A setup utilizing a Raspberry Pi camera module as a light sensor was built to execute such measurements and in this study, we are extending the accuracy and practicality of the setup.

The inspected samples are purified via an Al_2O_3 column i.e. filtered through a fine-grained material in order that impurities are caught by the material but LAB itself goes through it. This method gets rid of the polar impurities, molecules with positively and negatively charged sides, that might be presented in the samples. A point of interest is also how the purification process affects the samples: filtering the sample multiple times through the column gives us the insight how to optimize the process and get the most transparent sample.

Another effect that must be taken into account is quenching caused by oxygen in the samples. Oxygen has been proven to decrease the intensity of light going through LAB [11]. Removing oxygen from the samples and performing the measurement for oxygenless samples gives a reference how the transparency could be improved by removing the quenching agent.

2 Liquid scintillation counting

The operating principle of scintillation counting is based on a specific material, a scintillator, transforming kinetic energy of incident radiation to light pulses. These light pulses are converted to electric signals which give information about the energy of the reaction. Liquid scintillator counters have nearly a linear relationship between the energy deposited and the number of scintillation photons. Since photomultipliers are also linear devices the electrical signal will be also proportional to the reaction energy. A great advantage of liquid scintillation counters is good time resolution. Scintillation process is fast, typically of the order of nanoseconds. This property is thus an advantage in cases where a separation of two particles is needed. [1]

The scintillator used for detection can be either solid, liquid or gaseous, and inorganic or organic. Solid scintillators are for example sodium natrium crystal and different kinds of plastics. Counters utilizing solid scintillators have high gamma radiation detection efficiency but lack in detecting lower energy radiation like alpha and beta. Radiation must be of high energy to penetrate the scintillators surface which means that lower energy particles lose their energy before entering the scintillator. Liquid scintillator counters, on the other hand, can be used to detect other than gamma radiation since the radioactive material is mixed with the scintillator. [1]

2.1 Measuring light

Eyesight is one of our senses that we use to observe our environment and phenomena happening around us. It is based on our ability to sense light, and that is what scintillation detectors basically do. Light is electromagnetic radiation that covers only a small portion of the whole electromagnetic spectrum, shown in Figure 2. This range falls between ultraviolet and infrared ranges, approximately between 360 nm and 830 nm [12]. The boundaries between these different types of radiation are uncertain since the human eye is insensitive to light at $360 - 410$ nm and $720 - 830$ nm and for some people eyes do not register light at these wavelengths at all. For this reason, the wavelength range of light may differ from source to source, being defined for example from 400 nm to 750 nm.

Measuring light is not a straightforward process. Scattering, absorption, and reflection of light have an impact on optical system and must be taken into account when the amount of light is measured. Scintillation detectors for weakly

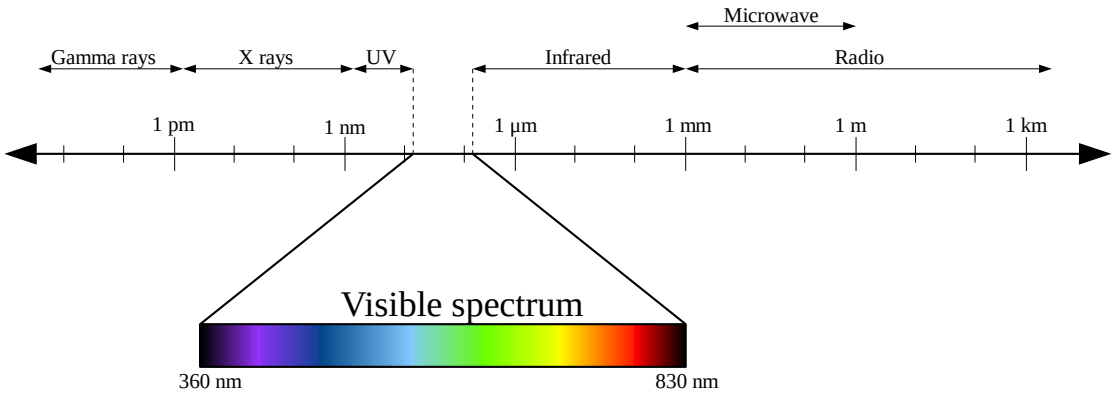

Figure 2: The spectrum of electromagnetic radiation. The visible spectrum, wavelengths human beings are able to see, is only a small part of the whole electromagnetic spectrum. Reference for the picture taken from [12].

interacting particles such as neutrinos must have large volumes in order to detect a significant number of particles. Attenuation length indicates how large detector can be built using liquid scintillator in question.

2.1.1 Photometric quantities

Radiometry is a branch of physics that focuses on measuring electromagnetic radiation [12]. Some important quantities that describe electromagnetic radiation are radiant flux Φ_e, radiant intensity I_e, irradiance E_e, and radiance L_e. Radiometry applies to all wavelengths of electromagnetic radiation but photometry is usually applied when talking about light. Before going through the photometric quantities there is need to discuss how human eye responds to light.

Our eyes have two kinds of light receptors: rods and cones. The rods are responsible for our night vision since they only react to low light levels. This is the so-called scotopic vision. The cones in the other hand work in the daytime and give us the ability to see color. The cone vision is called photopic vision. The response to light is not the same for different wavelengths. The spectral sensitivity is highest at the wavelengths of green color and drops at higher and lower wavelengths. Although the spectral response varies from person to person, the standard response curve for photopic vision has been adopted. This is the standard luminosity function (or spectral luminous efficiency function) $V(\lambda)$, represented in Figure 3. [12]

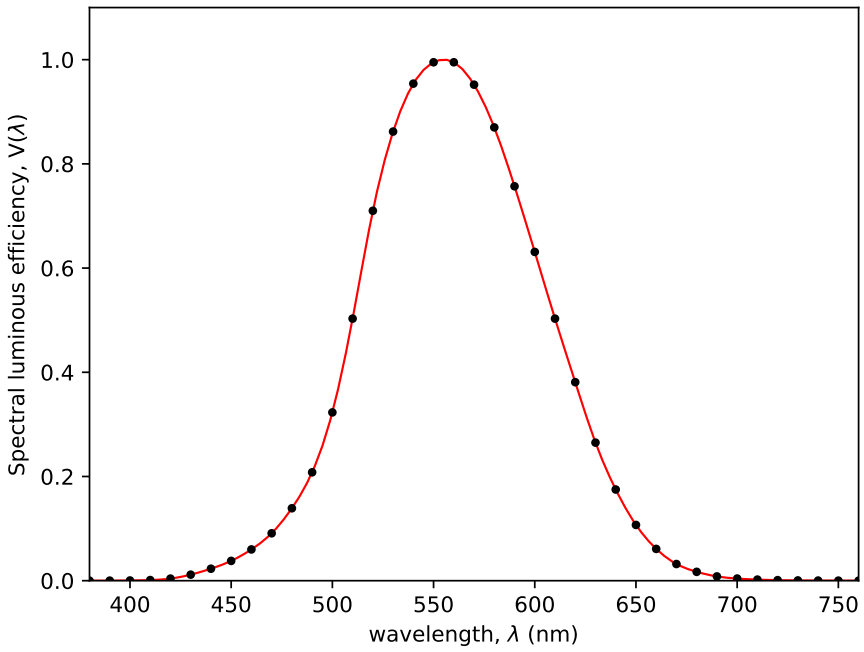

Figure 3: Spectral luminous efficiency function as it was defined in 1924 by the International Lighting Commission CIE. The curve peaks around 555 nm which means that human eye is the most sensitive to green color. Data points are taken from [12].

Photometry concerns only the visible portion of the electromagnetic spectrum, that is wavelengths between 360 and 830 nm. As in radiometry, there are similar quantities in photometry characterizing light: luminous flux Φ_v, luminous intensity I_v, illuminance E_v, and luminance L_v. In fact, these quantities are their radiometric counterparts weighted with the standard luminosity function $V(\lambda)$. For example, the luminous flux [12] is defined as follows:

$$\Phi_v = 683 \int_{380}^{770} \Phi_e V(\lambda) d\lambda, \tag{2}$$

where Φ_e is radiant intensity at wavelength λ. The values of $V(\lambda)$ below 380 nm and over 769 nm are usually not included in photometric calculations due to them being small. This is why the integral boundaries go from 380 nm to 770 nm.

The other quantities are defined in the same manner, replacing Φ_e and Φ_v with different radiometric and photometric quantities in Equation 2. Therefore if we denote the radiometric quantities with Q_e and the photometric counterparts with Q_v we get a general equation [12]

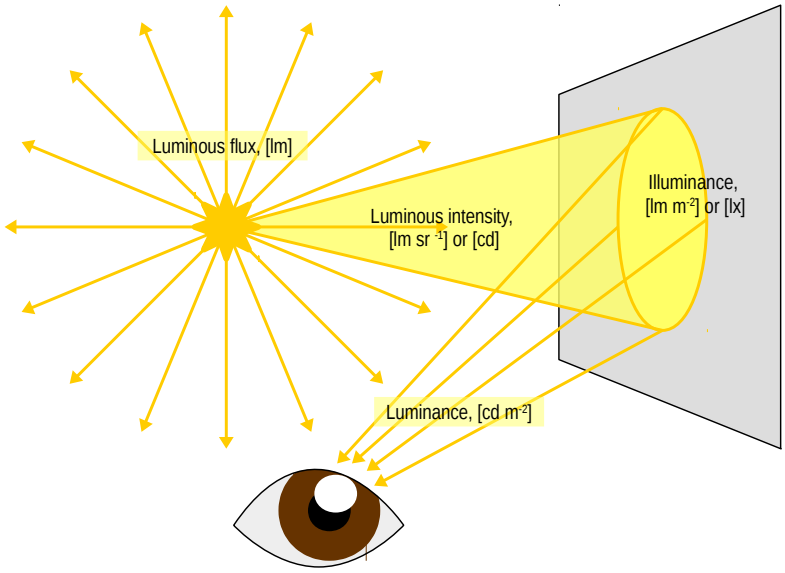

Figure 4: An illustration of a point-like light source that illuminates evenly in every direction. The yellow arrows around the light source represent luminous flux whereas the light cone to the paper is luminous intensity. Illuminance is the amount of light that hits the surface i.e. the light spot on surface and luminance is the light emitted from the surface. Reference from [13].

$$Q_v = 683 \int_{380}^{770} Q_e V(\lambda) d\lambda. \tag{3}$$

The integration bounds are the range of visible light. Factor 683 is the luminous efficacy of monochromatic radiation at the wavelength 555 nm. Luminous efficacy is discussed further on. Now that the four photometric quantities are defined they can be discussed in detail.

Luminous flux Φ_v is the perceived power of light. The SI unit of luminous flux is lumen [lm]. Luminous flux from a point per unit solid angle in a specific direction is luminous intensity. The solid angle is given in steradians and hence the unit for luminous intensity is lumens per steradian [$\mathrm{lm\,sr^{-1}}$]. This unit is also known as candela [cd].

Illuminance and luminance are tied to the area of which the light is cast upon. Illuminance is how much the incident light illuminates a surface i.e. the total flux on the surface. Its unit is [$\mathrm{lm\,m^{-2}}$] which is commonly denoted as [lx]. Luminance, on the other hand, is the amount of light that is emitted from the surface (luminous intensity per area unit) and therefore its unit is [$\mathrm{cd\,m^{-2}}$]. Figure 4 shows photometric quantities for a pointlike light source that illuminates constantly in every direction.

As the luminous quantities can be obtained from the corresponding radiant values applying equation (3), a similar set of equations can be derived to convert the photometric quantities to the radiant quantities [12]:

$$Q_e = \int_0^\infty Q_v V(\lambda) d\lambda. \tag{4}$$

In this case, the integration boundaries go from 0 to ∞, as radiometric quantities can be applied to every wavelength.

Previously mentioned luminous efficacy K is an important concept when converting luminous quantities to radiant ones and vice versa. Rather than being an actual efficacy luminous efficacy tells how efficiently a radiating source produces visible light. It is not a dimensionless quantity but its unit is [$\mathrm{lm\,W^{-1}}$]. Luminous efficacy [12] is defined as

$$K = \frac{Q_v}{Q_e}. \tag{5}$$

Manufacturers offering lightning solutions aim at higher and higher luminous efficacy which means more energy efficient products. Ideally, the greatest luminous efficacy is already mentioned 683 $\mathrm{lm\,W^{-1}}$ in Equations 2 and 3 that can be reached at 555 nm. A lamp or a LED emitting only green light at one wavelength would not be ideal for illumination and would not even be possible due to their continuous spectrums. Additionally, some amount of the energy always dissipates as heat which lowers the luminous efficacy. For example, a measured luminous efficacy for a low voltage halogen lamp (60 W) is 25.6 $\mathrm{lm\,W^{-1}}$, for a fluorescent lamp (54 W) 81.6 $\mathrm{lm\,W^{-1}}$, and for a white LED (16 W) 150.5 $\mathrm{lm\,W^{-1}}$ [14].

2.1.2 Optical properties of materials

When radiation passes through a material, was it solid, liquid or gas, the flux of the radiation will decrease via various ways. Transmittance $\mathrm{T}(\lambda)$ denotes how efficiently the material transmits radiation: it is the ratio of transmitted radiant or luminous flux to the incident flux [12]. The transmission of light differs widely depending on the material. Some materials may have high transmittance in the visible spectrum but may lack in ultraviolet and/or infrared spectrum. Figure 5 shows transmission curves of fused silica and acrylic. As seen in

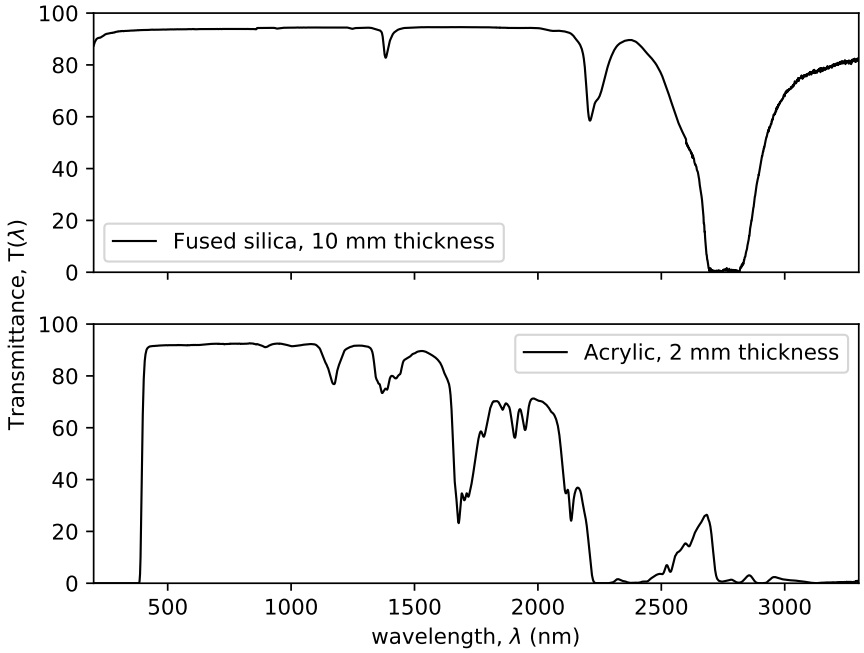

Figure 5: Transmission curves between 200 nm and 3300 nm for two optical substrates commonly used in optical applications, fused silica (upper curve) and acrylic (lower curve). Both materials transmit light well at certain wavelengths despite the small difference between thickness. However, acrylic does not let radiation from deep UV range to pass and therefore is not suitable UV applications. The data received from Thorlabs [15].

the figure, acrylic works well for visible light but fused silica can also be used in UV applications.

The reduction in transmittance happens via several processes. The amount of absorption and scattering depend on how long distance light travels in the medium. A central point in our study is to determine the attenuation caused by these two processes. Other processes associated with light are refraction and reflection. These processes happen in the boundary of two media and depend on the direction of the incident light ray. In our measurements, the light beam passes through several different media and therefore a review of their impact is also in place.

Absorption and scattering

In absorption process, the energy of a photon is transferred to another particle, for example to an electron. The energy dissipates as heat. The magnitude of absorption depends on the constitutes of the material and the wavelength of the photons. As mentioned before, fused silica is used in measurements involving radiation from UV range instead of regular glass. Fused silica ideally contains

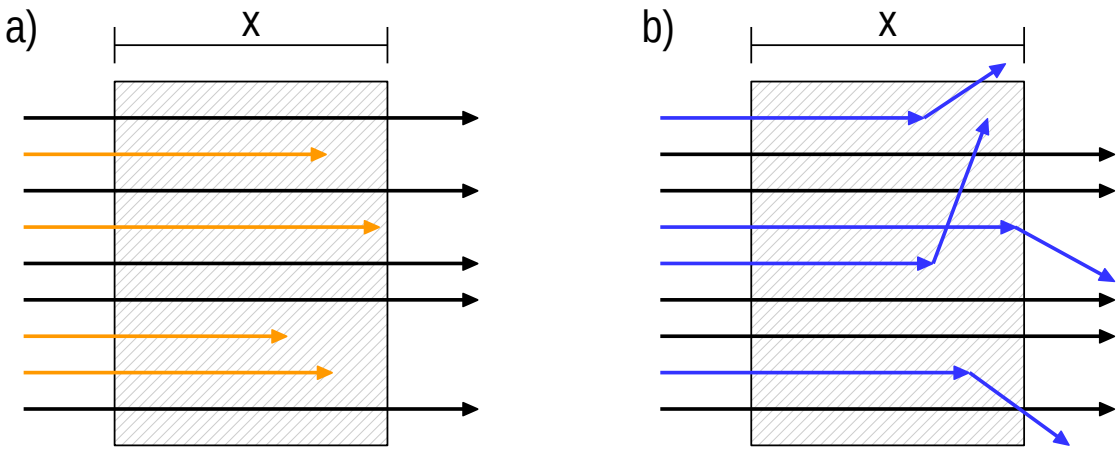

Figure 6: Schematic picture of two main processes that contribute to light attenuation. In picture a) photons are absorbed by the medium (orange arrows) and in picture b) photons scatter from the molecules of the medium (blue arrows). Reference for the picture from [16].

only SiO_2 whereas glass is SiO_2 mixed with other chemical compounds such as Na_2O, CaO, and B_2O_3. Added compounds lower the high melting point and viscosity of pure SiO_2, thus easing the production of glass. However, this has an effect on the optical properties: the added compounds absorb effectively UV radiation.

Scattering is a physical process where the loss of flux is caused by photon changing its course upon colliding with another particle. In addition, the energies of the particles might change in the process, having an effect on the velocity and momentum of the particles. For photons important scattering processes include Rayleigh scattering and Mie scattering.

Rayleigh scattering occurs when light scatters from a particle or a molecule that is much smaller than the wavelength of the light. This concerns particles with sizes smaller than a tenth of the wavelength of the light. The intensity of the scattered light is related to wavelength [17]

$$I \propto \lambda^{-4}. \tag{6}$$

Rayleigh scattering thus has a strong wavelength dependence, being inversely proportional to λ^4. The shorter wavelengths of the light spectrum are therefore enhanced. This causes, for example, the sky to appear as blue.

When the molecule where the light scatters is bigger than the wavelength of the light, Mie scattering is a more dominant process. Mie scattering process does not have a strong wavelength dependence like Rayleigh process has but

it depends on the size of the particle contributing to the collision. PPO and bis-MSB in many cases contain suspended particles or even radioactive traces. These particles cause incident photons to Mie scatter in the scintillator mixture and thus decrease the overall light intensity. While Rayleigh scattering is non-avoidable process since the scattering happens mainly on bound electrons Mie scattering can be avoided or minimized by reducing the number of suspended particles in the mixture. [18]

The attenuation of light caused by absorption and scattering processes is related to the properties of the medium via Beer-Lambert law [19]. The law states that

$$A(\lambda) = \log_{10} T(\lambda) = \mu_{10}\ell, \tag{7}$$

where I_0 and I are the intensities of the beam entering and leaving the medium, μ is the (decadic) attenuation coefficient of the medium, and ℓ is the thickness of the medium. $A(\lambda)$ is absorbance, a commonly used quantity in chemistry.

Equation (7) can also be written by the means of intensities of light. Transmittance can be written as the ratio between transmitted and initial intensities. Changing the decadic logarithm to natural logarithm yields the following relation:

$$\frac{\log(I/I_0)}{\log 10} = \mu_{10}\ell. \tag{8}$$

Multiplying μ_{10} with $\log 10$ yields the attenuation coefficient μ. The attenuation coefficient is the inverse of the attenuation length L and thus (8) can be written as

$$I = I_0 \mathrm{e}^{-\frac{\ell}{L}}. \tag{9}$$

The attenuation length is the distance in a material where the flux of the light beam has dropped to $1/\mathrm{e}$ (≈ 63 %) of its incident flux.

An attenuation length of approximately 25 m has been measured for LAB based liquid scintillators at the wavelength of 430 nm. Goett et al. [20] measured attenuation lengths for purified LAB, LS (LAB + BPO + bis-MSB), and LS doped with gadolinium at several wavelengths. They got 28.6 m for pure LAB and 24.6 m for LS at 430 nm. A more recent study by Yang et al. [21] an attenuation length of 25.8 m at 430 nm was measured.

Because attenuation length depends on both absorption and scattering it can be separated to absorption length and scattering length. This allows examining the impact of both processes individually. Attenuation length is denoted by absorption length L_{abs} and scattering length L_{sca} as [22]

$$\frac{1}{L} = \frac{1}{L_{\text{abs}}} + \frac{1}{L_{\text{sca}}}. \tag{10}$$

A detector that has PMTs in every direction can collect also the scattering photons and thus scattering does not necessarily degrade the energy resolution of the detector. However, the energy resolution of the detector suffers from a short absorption length. Absorption length is difficult to determine directly but it can be deduced from measured attenuation and scattering lengths using Equation (10). Zhou et al. [22] measured the scattering length of approximately 30 m for linear alkylbenzene used in JUNO detector. With a value of 20 m for attenuation length of LAB, the absorption length of LAB was determined to be approximately 60 m. In these circumstances the needed energy resolution for JUNO detector[1] to measure the mass hierarchy of neutrinos is satisfied. [22]

Refraction and reflection

Measuring light through liquids is not as simple as through solids: there is always other media besides the liquid that light needs to pass through. In the case of this study, the container of LAB causes also attenuation. To find out the attenuation that is due to LAB the effect of the container needs to be subtracted from the overall attenuation. Unfortunately, this cannot be done by measuring an empty container and removing the results from results of a measurement with liquid added to the container. This is because light behaves differently when encountering solid-to-solid or solid-to-air boundaries.

The behavior of light in interfaces can be explained simply by the well-known Snell's law, also known as the law of refraction. The law relates the properties of a light ray going through two media to the refractive indexes of said media [12]:

$$n_1 \sin\theta_1 = n_2 \sin\theta_2 \tag{11}$$

n_1 and n_2 are the refractive indexes of medium 1 and medium 2 and θ_1 and θ_2 are the angles between light rays and the normal of the interface between the media.

[1] The required energy resolution for JUNO is $3\ \%/\sqrt{\text{MeV}}$ which means that the minimum of 1200 photons per MeV needs to be detected by the PMTs. [22]

As we can see from Equation (11) the direction of the light rays in medium 2 depends on which angle they penetrate the interface. This refraction phenomenon is non-existing when $\theta_1 = 0$. Even if every single photon was so well collimated that every one of the photons hit the interface perpendicularly they would scatter from the molecules in both media and change their course.

A couple of examples using Equation (11) make it clearer why the intensity of light is less through air than a liquid. Consider a light ray that comes from air and goes to acrylic at an angle of $\theta_1 = 30^\circ$. The refractive index of air is approximately $n_{\text{air}} \approx 1$ whereas acrylic has $n_{\text{acrylic}} \approx 1.5$ (at $\lambda = 430$ nm) [23], hence the light ray refracts

$$\begin{aligned}\theta_{\text{acrylic}} &= \arcsin\left(\frac{n_{\text{air}}}{n_{\text{acrylic}}}\sin\theta_1\right)\\ &= \arcsin\left(\frac{1}{1.5}\sin 30^\circ\right)\\ &= 19.47^\circ.\end{aligned}$$

Now as the light ray continues to leave the acrylic and enters inside the container the amount of refraction depends on whether there is liquid or gas. First, consider the situation where the light ray travels to LAB ($n_{\text{LAB}} = 1.488$ at $\lambda = 430$ nm [23]) from acrylic. This time the light ray refracts

$$\begin{aligned}\theta_2 &= \arcsin\left(\frac{n_{\text{acrylic}}}{n_{\text{LAB}}}\sin\theta_{\text{acrylic}}\right)\\ &= \arcsin\left(\frac{1.5}{1.488}\sin 19.47^\circ\right)\\ &= 35.88^\circ.\end{aligned}$$

The situation in which the liquid is substituted with air can be calculated in similar fashion. In this case, the refraction angle is $\theta_3 = 60.7^\circ$. Both situations are presented in Figure 7.

Even though the angles may be a bit exaggerated the outcome is clear: the light disperses to a wider area when there is no liquid in the container. This means that less light reaches the small camera sensor at the other end of the container and it looks like the light intensity decreases more through air than liquid.

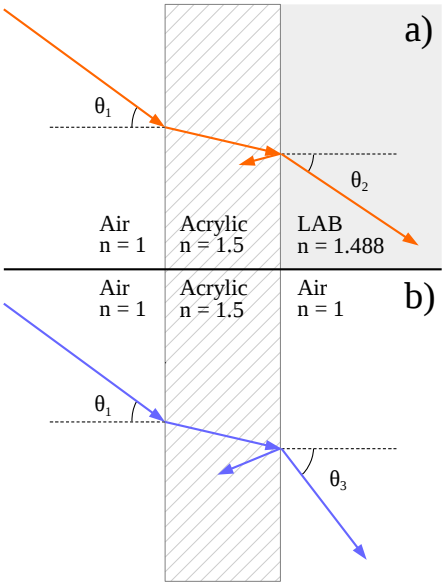

Figure 7: Illustration how light behaves at different interfaces. A single light ray hits the surface of acrylic in the same angle θ_1 in both situations a) and b). However, the light ray refracts and reflects less in the situation a) than in the situation b): light rays refract θ_2 and θ_3 degrees respectively so that $\theta_2 < \theta_3$.

Besides refraction reflection also plays a part in the propagation of light. Total internal refraction is tied to the critical angle θ_c. Light rays hitting the surface with a bigger angle than the critical angle are fully reflected back to the medium 1 and do not penetrate the surface. Critical angle can be derived from Equation (11) setting $\theta_2 = 90°$:

$$\theta_c = \theta_1 = \arcsin\left(\frac{n_2}{n_1}\sin 90°\right) = \arcsin\frac{n_2}{n_1}. \tag{12}$$

Internal reflection occurs only when the light travels to a medium with a smaller refractive index, in this situation the inner surface of the container. Critical angle when light goes to LAB is

$$\theta_c = \arcsin\frac{1.488}{1.5} = 82.75°,$$

and when light travels from acrylic to air the critical angle is $\theta_c = 41.81°$. The smaller critical angle of the acrylic-air interface compared to the critical angle of acrylic-LAB interface indicates that light tends to reflect more at the former interface. This further on decreases the overall photon flux.

Refraction and reflection need to be taken into account also in scintillator counters. To decrease the effect, materials with a refractive index similar to the scintillators refractive index are used. Solid scintillators are connected to light guides, optical fibers, and PMTs via optical cement or glue, depending on the situation. For liquids the choice of container material is crucial. Acrylic is commonly used since it is a light material that has light transmission of 92 % and refractive index that matches well with LAB [23].

2.2 Liquid scintillator materials

Liquid scintillator mixture is mainly composed of an organic solvent. When a particle enters the scintillator mixture its energy transforms into heat, ionization, and excitation of solvent molecules. Solvents are aromatic compounds that have one or more ring-shaped benzene structures. These compounds have free valence electrons that are not associated with any particular atom in the molecule. Transitions made by the free electrons lead to the process of scintillation.

While energy is exchanged between solvent molecules it may excite so-called scintillator or fluor molecules. A scintillator is a fluorescent material that emits photons in the region of visible light when the excitation discharges. Emitted photons are collected with photosensors. Sometimes the emitted photons do not match well with the sensitivity of chosen photosensor. This is corrected by adding wavelength shifter to the cocktail that emits absorbed photons with a longer wavelength. Wavelength shifter thus improves the counting efficiency of the detector. [1]

Light emission from a scintillation material happens due to photoluminescence. Photoluminescence is one of the various types of luminescence, spontaneous emission of radiation from electronically or vibrationally excited molecules or atoms. The excitation may be caused for example by ionizing radiation (radioluminescence) or by heat (thermoluminescence). A more familiar example may be the light produced by living organisms such as fireflies and some deep-sea fish called bioluminescence, a form of chemiluminescence that is the emission of light caused by chemical reaction. [19]

Concerning photoluminescence, the excitation is due to absorption of light. Photoluminescence is usually distinguished between fluorescence and phosphorescence. Fluorescence occurs in transition from the singlet electronic state S_1 back to the singlet ground state S_0. Phosphorescence, on the other hand, might occur when the molecule undergoes intersystem crossing, a nonradiative

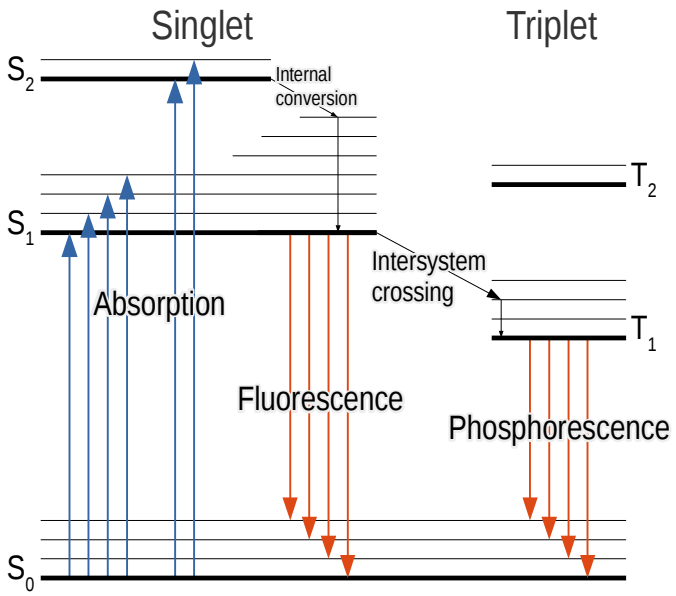

Figure 8: Triplet and singlet energy levels of an organic molecule. The levels marked with S and T are the electronic states and others are vibrational states. Due to absorption, the electron moves to an excited state. The light emission is either fluorescence or phosphorescence. Picture adapted from [19].

transition to an electrical or vibrational state of a different spin multiplicity. After that, the de-excitation from the triplet state T_1 to the singlet ground state S_0 is accompanied by phosphorescence. Figure 8 depicts the excitations and relaxations of different states. [19]

Scintillation light is mainly produced in the transition $S_1 \rightarrow S_0$ in the form of fluorescence. Phosphorescence in a solution at room temperature is less likely than a nonradiative relaxation of T_0 [19]. Transition $S_2 \rightarrow S_0$ is forbidden since the so-called Kasha's rule [19] states that the photon emission occurs only from the lowest excited state that is S_1[2].

One important quality of a good scintillator material is that it does not absorb the light it has emitted. This means that the less absorption and emission spectra overlap the more emission light is produced. Emission spectra of fluorescent materials in many cases are slightly shifted to higher wavelengths than their corresponding absorption spectra, as seen in Figure 9. This so-called Stokes shift [19] happens because of the vibrational excitations. The molecule absorbs light in such way that it excites a vibrational state. The relaxation from vibrational state to S_1 happens via internal conversion that is a nonradiative transi-

[2]Although $S_2 \rightarrow S_0$ is forbidden there exists compounds that de-excite this way. One of these compounds is a blue colored organic compound called azulene. [19]

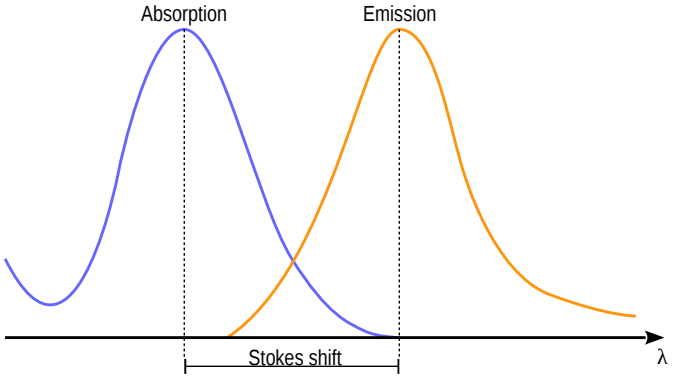

Figure 9: Stokes shift between absorption and emission spectra. Picture adapted from [19].

tion like intersystem crossing (Figure 8). This means that when the relaxation S_1 to S_0 occurs the emission energy is lower than absorbed quantity and therefore the wavelength is longer.

Following sections concentrate on linear alkylbenzene (LAB) as a solvent and 2,5-Diphenyloxazole (PPO), a fluor used in scintillator mixtures. Since the purification of the scintillator solvent samples is also a point of interest in this study a review of different purification methods is also provided.

2.2.1 LAB

The samples in question belong to a group of an organic compound called **l**inear **a**lkyl**b**enzene (LAB) [25]. The chemical formula (Figure 10) for LAB is $C_6H_5C_nH_{2n+1}$ where n can range from 10 to 16. It consists a benzene which is a

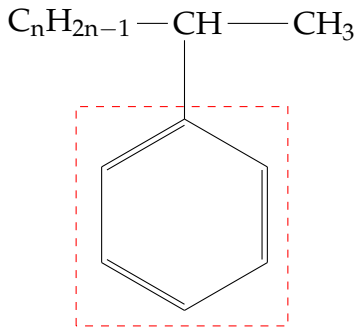

Figure 10: The chemical formula of linear alkylbenzene. The benzene structure, a common factor between different liquid scintillators is circled with the red dashed line. The alkyl chain may be attached to the benzene also from other carbon atoms of the chain. Reference is taken from [24].

Table 1: Physical and chemical properties of linear alkylbenzene [24].

Density	$0.858 - 0.862\ \mathrm{g\,cm^{-3}}$
Boiling temperature	$280 - 311\ ^{\circ}\mathrm{C}$
Flash temperature	$147\ ^{\circ}\mathrm{C}$
Hydrogen atoms	$6.2910 \times 10^{22}\ \mathrm{cm^3}$

common trait among liquid scintillator solvents. LAB is mainly used as an intermediate in the production of **l**inear **a**lkylbenzene **s**ulfonate (LAS) that is a major component of many household detergents. LAB is commercially produced by alkylation of benzene, simply put, attaching an alkyl chain to a benzene ring. Paraffins are used as the feedstock in this process. [26]

LAB is a promising liquid scintillator solvent because of its favorable properties. LAB is a transparent liquid that has a very high flash point and low toxicity. Because it is so widely used in the petrochemical industry it is produced in large quantities and can thus be purchased at reasonable price. It doesn't damage acrylic, a suitable material for liquid scintillator vials because of its high optical transparency. LAB itself has a long attenuation length: measured attenuation length is more than 20 meters depending on the wavelength of the light [20]. Some physical and chemical properties of LAB are given in Table 1.

Many neutrino experiments relying on liquid scintillation counting have used 1,2,4-trimethylbenzene, also known as **p**seudo**c**umene (PC), as a solvent. Other commonly used solvents include 1,2-dimethyl-4- (1-phenylethyl)-benzene (or phenyl-*o*-xylythane, PXE), mesitylene, dodecane, and BC521. Out of these chemicals, PC gives highest light output and is thus the most widely used solvent in neutrino experiments. However, it is highly toxic to the human body and harmful to the environment. In addition, it has a low flashpoint of 48 °C which causes more safety concerns. For these reasons, effort has been put into finding substitutes to PC, and LAB is one of these candidates. [23]

2.2.2 PPO and additives

PPO (2,5-Diphenyloxazole) is an organic compound used commonly as a primary scintillator in liquid scintillator mixtures. PPO is a white powder under normal conditions and it consists two benzene rings attached to a rings structure containing nitrogen and oxygen atoms (Figure 11). It absorbs photons with a wavelength between $280 - 325$ nm and has an emission peak at 370 nm [18]. Although the light yield of PPO is around 20% smaller than the light yield of another commonly used primary scintillator called butyl-PBD (2-

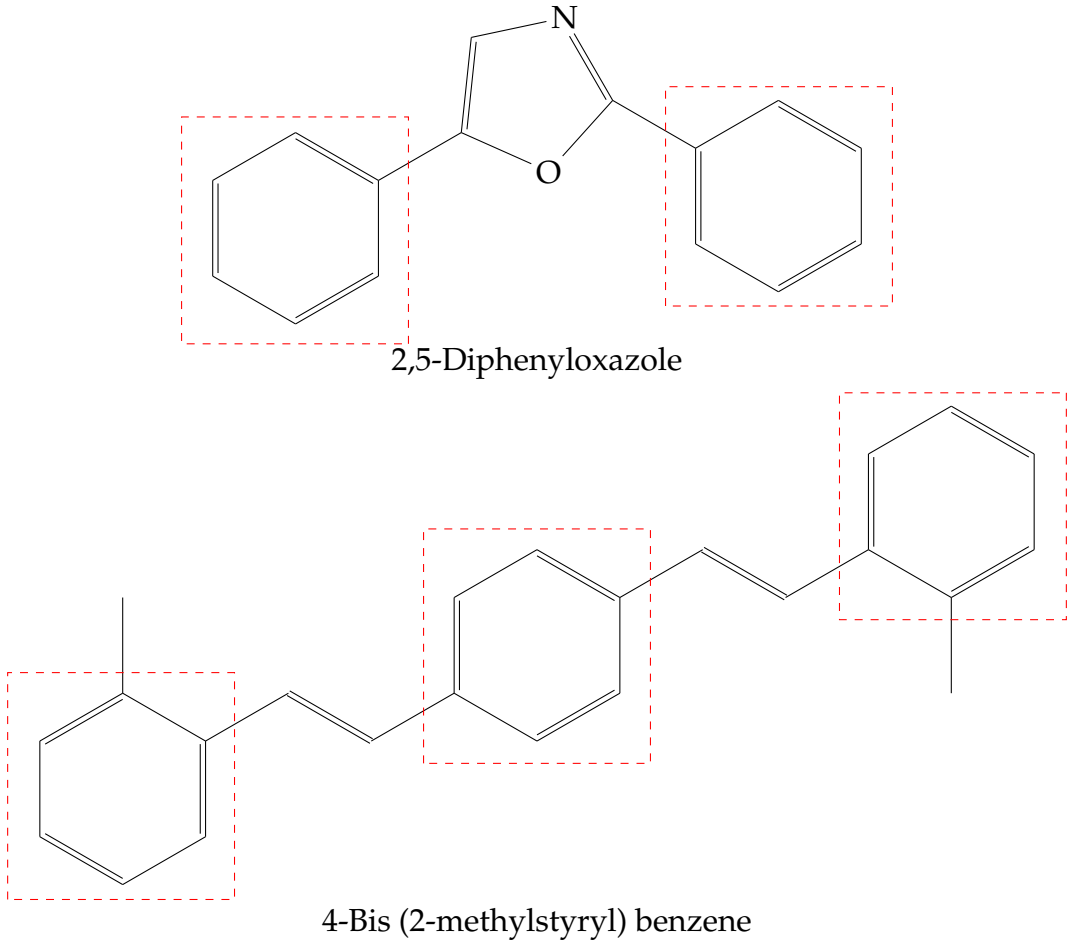

Figure 11: The chemical formulae of the scintillators. Upper formula represents the primary scintillator PPO and under it is the wavelength shifter Bis-MSB. Again, the benzene rings are featured in the compounds. These kinds of benzene ring chains have been proven to produce the best scintillation yield. The formulae are from [18].

(4-tert-butylphenyl)-5- (4-biphenyl)-1,3,4-oxadiazole). PPO's better solubility to solvent and lower price are reasons why it is usually chosen over butyl-PBD for applications with a large amount of liquid scintillator [27]. PPO is used for example neutrino experiments in SNO+ and JUNO, and also in C14 experiment.

Even though nowadays PMTs have better sensitivity to light near ultraviolet wavelengths some PMTs have the highest detection efficiency at around 400 nm. Therefore wavelength shifters are still used to improve the scintillation yield and are necessary for large-volume applications. Wavelength shifters re-emit lower energy photons which means light at longer wavelengths. Common wavelength shifters include POPOP (1,4-bis (5-phenyl-2-oxasoly) benzene) and

Bis-MSB (4-Bis (2-methylstyryl) benzene). These compounds have been studied as a part of a scintillator mixture using LAB as solvent and PPO as primary scintillator by Nemchenok et al. [24]. Both mixtures turned out to have similar light yields, attenuation lengths, and energy resolutions, having difference in emission wavelengths. POPOP has emission maximum emission peak around 410 nm whereas the emission peaks of Bis-MSB is at higher wavelengths, around 430 nm. Hence the choice of the wavelength shifters depends on the sensitive region of PMTs in use. For example, the detector in JUNO experiment will use Bis-MSB in the scintillator mixture because the emission spectrum of Bis-MSB matches better with the PMTs in use [7].

Besides organic scintillators small amount of gadolinium ($0.1 - 0.2\%$ by weight) is sometimes added to the scintillator mixture in neutrino experiments [28]. Gadolinium (atomic number $Z = 64$) is a metal and its addition enhances the neutron-capture signal because of gadolinium's large (n, γ) cross-section. Neutron-capture is one way to identify an inverse β-decay reaction mentioned in Section 1.1. Experiments taking advantage of gadolinium-loaded liquid scintillators are for instance RENO (**R**eactor **E**xperiment for **N**eutrino **O**scillations) experiment [29] studying neutrinos emitted from Yonggwang power plant in South Korea and former CHOOZ experiment [30] with its successor Double CHOOZ [31] in Chooz, France.

2.2.3 Purification

Liquid scintillator mixtures are known for being sensitive to environmental conditions. UV-light, oxygen and elevated temperatures cause changes in mixtures that can be observed as a yellowish color change of the liquid. This affects negatively to the transparency of the scintillator and thus deteriorates the overall light yield. For this reason, one must pay attention to preservation conditions and purification of the liquid scintillators.

Purification is needed to diminish scattering and absorption caused by suspended particles. Three purification methods have been described more in detail in [7] and [18]:

Vacuum distillation The fact that different compounds have different boiling points can be used to separate the impurities from scintillator mixture. Because the liquids often have low flash point decrease in the boiling point of the liquid is needed. This is done by exposing the liquid mixture to low pressure and heat. However, this technique has been proven to be challenging to perform: too high temperature may break chemical bonds

of the scintillator molecules and this leads to different scintillation properties. Additionally, distillation should be performed before any mixing of the components since their different boiling points complicate the process.

Water extraction The scintillator is mixed well with water to ensure that polar impurities will attach to the polar water molecules. When the scintillator mixture components and water (containing the impurities) separate to two different layers of liquid the latter can be disposed of. This method efficiently removes metal ions like radium (96.5 % removal) and lead and polonium (82–87 % removal) [7].

Column chromatography Using a column to purification means that the liquid is poured into a long column containing fine purification material and let pass through it. While the liquid goes through the column the impurities will stay within the purification material. Reliable purification materials in use are aluminum oxide Al_2O_3 and silica gel Si_2O. Both are white powders having a grain size between 40–90 micrometers [18]. This method has been proven to increase attenuation lengths of LAB samples greatly [7] but it is also quite time-consuming.

Column chromatography is used also in our LAB study. A filtering paper and glass fiber are placed to the bottom of the column to prevent the purification material (Al_2O_3 in this case) to come through the separating funnel. It is advisable to wear safety glasses and respirator mask while preparing the column because dust clouds of Al_2O_3 may be formed during the preparation.

Degasification Degasification is performed when a liquid is wanted to be stripped out of a certain gas. It is performed using an inert gas such as nitrogen or argon that substitutes the unwanted dissolved gas. In our case, the LAB samples are bubbled with nitrogen in order to remove oxygen present in the samples. An increase of 11% in light yield has been observed by Xiao et al. [11] in samples from which the oxygen has been removed.

3 C14 experiment

C14 experiment aims at finding liquid scintillator based on LAB with $^{14}C/^{12}C$ -ratio smaller than 10^{-18}. ^{14}C causes the main background in low energy measurements with organic scintillators and thus has an effect on the sensitivity of the measurements. Besides 14C experiment in Pyhäsalmi an experiment in Baksan, Russian also focuses on determining the isotopic ratio of LAB based scintillator.

Pyhäsalmi Mine has been hosting physics experiments since the establishment of CUPP (**C**entre for **U**nderground **P**hysics in **P**yhäsalmi) in the middle of 90's. EMMA (**E**xperiment with **M**ulti**M**uon **A**rray) has been running since 2003 and focuses on studying the composition of cosmic rays at the knee region ($1 - 10$ PeV) [32]. 11 detector stations operate in the depths of 45 and 75 meters. During site investigation for LAGUNA project, it was found that the infrastructure of the Mine is able to host a large-scale detector installations. Based on the investigations Lab 2 was built to the depth of $1,430$ m ($\sim 4,000$ m.w.e) [33] and at the moment the first experiment, C14 experiment, in the new hall is running.

Before going more deeply into the setup of C14 experiment a small review of why the presence of ^{14}C in organic scintillators is a problem and where does it originate from may be in place.

3.1 Origin of ^{14}C in organic scintillators

Carbon has three naturally occurring isotopes: ^{12}C, ^{13}C, and ^{14}C. Most common is ^{12}C with an abundance of 98.9 %. ^{12}C and ^{13}C both are stable isotopes but ^{14}C is radioactive with a half-life of $5,730$ years. Notably used in carbon dating, a method for determining the age of organic materials, ^{14}C is not as useful in measurements targeting on low energy processes. The reason is that it causes interfering background activity. ^{14}C decays via β^--decay to nitrogen:

$$^{14}_{6}\mathrm{C} \;\rightarrow\; ^{14}_{7}\mathrm{N} + \mathrm{e}^- + \bar{\nu}_{\mathbf{e}}. \tag{13}$$

The decay process causes typical beta spectrum with a maximum energy of $E_{\max} = 156$ keV. Since low energy experiments are focused on detecting rare events such as inverse beta decays or low-energy neutrino-electron scatterings the counts from decay process (13) may screen or pile up with these events.

On the surface of Earth ^{14}C is mainly produced because of cosmic rays: upon hitting the molecules of the atmosphere cosmic rays produce a flux of neutrons. These neutrons react with nitrogen producing radiocarbon via

$$n + {}^{14}_{7}N \rightarrow {}^{14}_{6}C + p. \tag{14}$$

Deep underground, at depths exceeding 300 m.w.e. [34] this production channel becomes less relevant as the Earth's crust decreases the flux of cosmic-ray particles. However, underground the elements among the bedrock contribute to the ^{14}C production. This is caused by alpha particles emitted from the uranium and thorium decay chains. Alpha particles react with surrounding elements such as Al, Mg, and Na forming neutrons. Neutrons again take part in several possible reactions which lead to the formation of carbon-14. These reactions include following [10]:

1. $n + {}^{17}_{8}O \rightarrow {}^{14}_{6}C + \alpha$
2. $n + {}^{14}_{7}N \rightarrow {}^{14}_{6}C + p$
3. $n + {}^{13}_{6}O \rightarrow {}^{14}_{6}C + \gamma$
4. $\alpha + {}^{11}_{5}B \rightarrow {}^{14}_{6}C + n$
5. direct ^{14}C emission from tripartition of ^{226}Ra

The order corresponds to the importance of the reaction in ^{14}C production. The contribution of the reactions caused by elements in the rock has been estimated for Borexino experiment and has given an isotopic ratio $^{14}C/^{12}C \sim 5 \times 10^{-21}$ [10] for petroleum (CH_2^-). This is much smaller than the measured value and they suggest that there might have happened ^{14}C contamination during the scintillator synthesis. Other reason might have been the scintillators exposure to CO_2. However, hydrocarbons used as a feedstock for liquid scintillators found underground have an isotopic ratio several orders lower than normal hydrocarbons. This is why underground oil sources are crucial for low-energy experiments depending on organic liquid scintillators. The source of hydrocarbons must be carefully chosen since the ^{14}C depends on the bedrock's uranium and thorium contents [33].

3.2 C14 experimental setup

As mentioned before, in ^{14}C experiment the isotopic ratio of several LAB samples is going to be determined. The measurement setup that contains a cylindri-

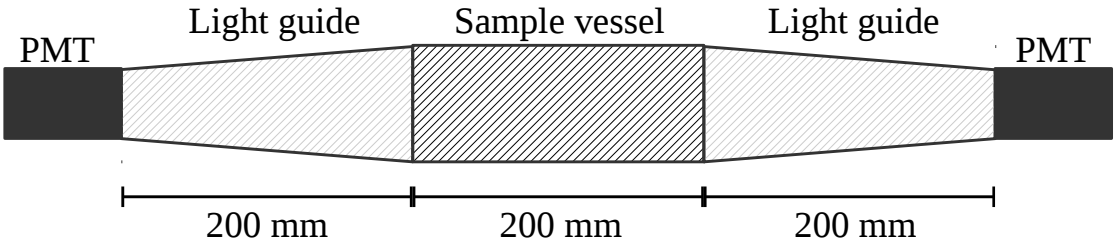

Figure 12: Illustration of the setup used in C14 experiment. The setup consists 1.6-liter vessel for the LAB sample, two light guides, and two photomultiplier tubes. Reference for the picture taken from [8].

cal vessel (V = 1.6 l) for the LAB samples, two acrylic light guides at each end of the vessel and two low-background photomultiplier tubes. The model of the PMTs is ET 9302B [8]. The diameter of the PMTs is 78 mm which is smaller than the diameter of the vessel. Consequently, the light guides are a bit narrower at the other end. The schematic drawing of the C14 detector setup is presented in Figure 12. Figure 13 shows underground laboratory hall (Lab 2) and the measuring station. The measuring station, Carbonarium, encloses the detector covered with thick layer of shielding against γ and neutron background, built from blocks of lead and copper [8].

Low-background measurements may also suffer from the decay products of radon. Radon is a radioactive element that is an intermediate step in decay chains of uranium and thorium. It occurs naturally in the gas phase and emits alpha particles when decaying. This makes it a harmful gas when inhaled. The amount of radon can be several times bigger underground than on the surface, depending on the nature of the bedrock. However, Lab 2 has an air exchange system that has dropped the radon activity concentration from 300 $\mathrm{Bq\,m^{-3}}$ to 50 $\mathrm{Bq\,m^{-3}}$ [33]. The radon level is further lowered by isolating the measurement setup from the laboratory environment i.e. radon inside Carbonarium decays.

To reach even lower radon levels clean air is flown to the inner parts of the detector. The air flow speed of the air feeding system is a bit less than 1 $\mathrm{l\,min^{-1}}$. The laboratory and Carbonarium both contain radon counters, and the radon concentration in the laboratory at the moment is 150 $\mathrm{Bq\,m^{-3}}$ and in Carbonarium 30 $\mathrm{Bq\,m^{-3}}$. The inner volume of the copper structure where the samples and PMTs are is flushed with 1 $\mathrm{l\,min^{-1}}$ of pressured air. This reduces the radon content within the system even further though it has not been determined how low as there is no radon counter inside the copper structure.

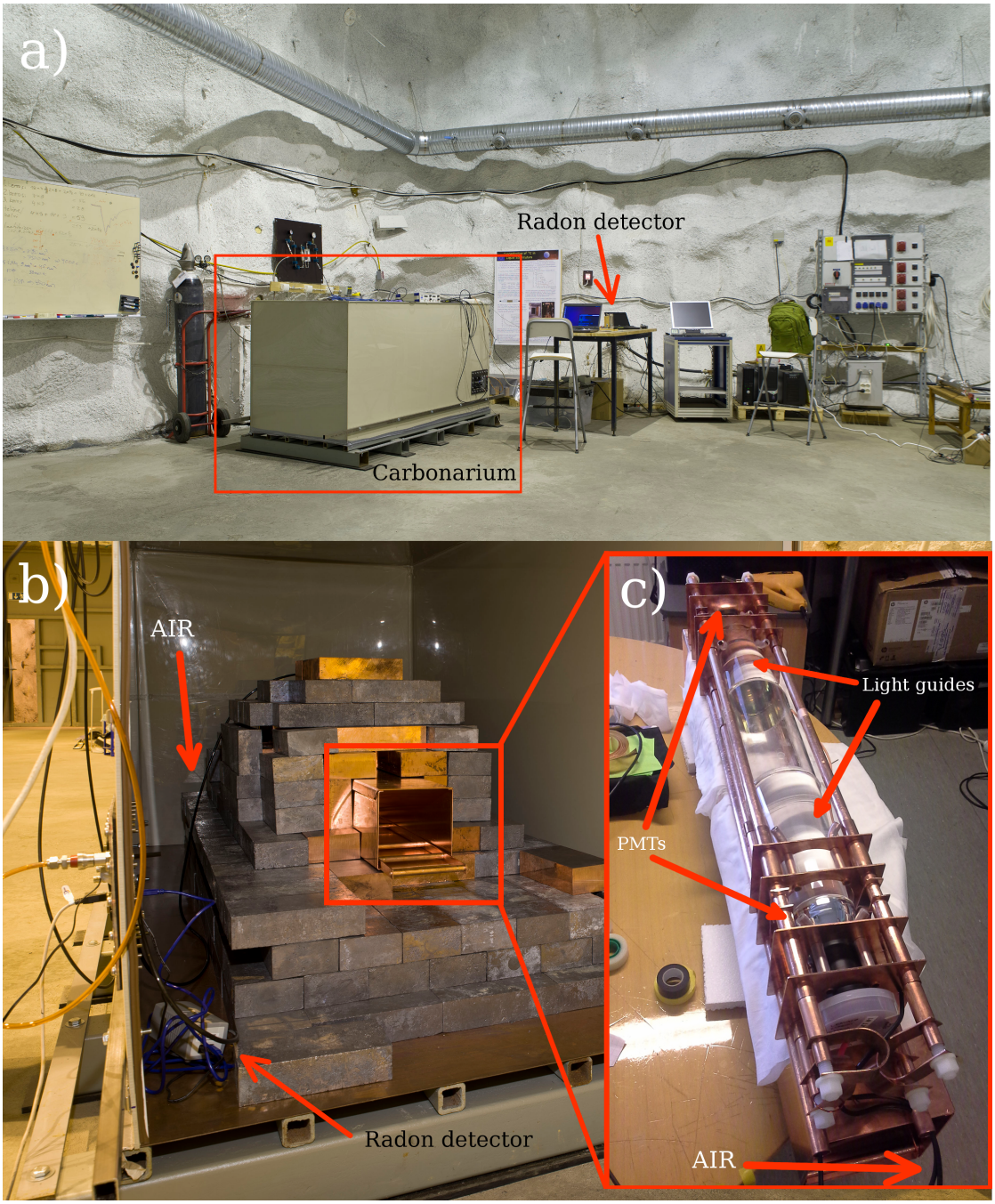

Figure 13: Photographs of C14 experiment measurement setup. Picture a) shows a part of CLAB Lab 2, located down below 1,430 m in Pyhäsalmi Mine. The measuring station Carbonarium can be seen entirely in the picture. An arrow points to a radon counter on the table that measures the radon level in Lab 2, that is around 150 $\mathrm{Bq\,m^{-3}}$. The lead and copper structure inside Carbonarium can be seen in Picture b). There is a radon counter inside Carbonarium as well, measuring the radon level inside it (30 $\mathrm{Bq\,m^{-3}}$). The scintillator sample and the PMTs are presented in Picture c). This setup goes into the copper structure where radon content is $< 30\ \mathrm{Bq\,m^{-3}}$ due to the air flushing. The air inputs are marked with arrow in Picture b) and Picture c).

4 Description of the light measurement setup

A small measuring apparatus using Raspberry Pi 3 single-board computer as the core component was built. The goal was to build a low-cost setup that could be used to determine the optical purity of various LAB samples. Because of such a long attenuation length, big setups are usually built to measure the attenuation length. For example, JUNO collaboration has measured the attenuation length of LAB using long tubes and PMTs to measure the light output.

4.1 General description

The frame of the apparatus is assembled using parts ordered from Edmund Optics. Four support rods (6 mm diameter, 200 mm length) and two circular mounting plates are used to build an optical cage system which ensures a sturdy frame where all the components can be placed in line. The optical cage has two other customized parts keeping it in place. The LED light source and the camera module are placed to each end of the apparatus. The measuring apparatus is

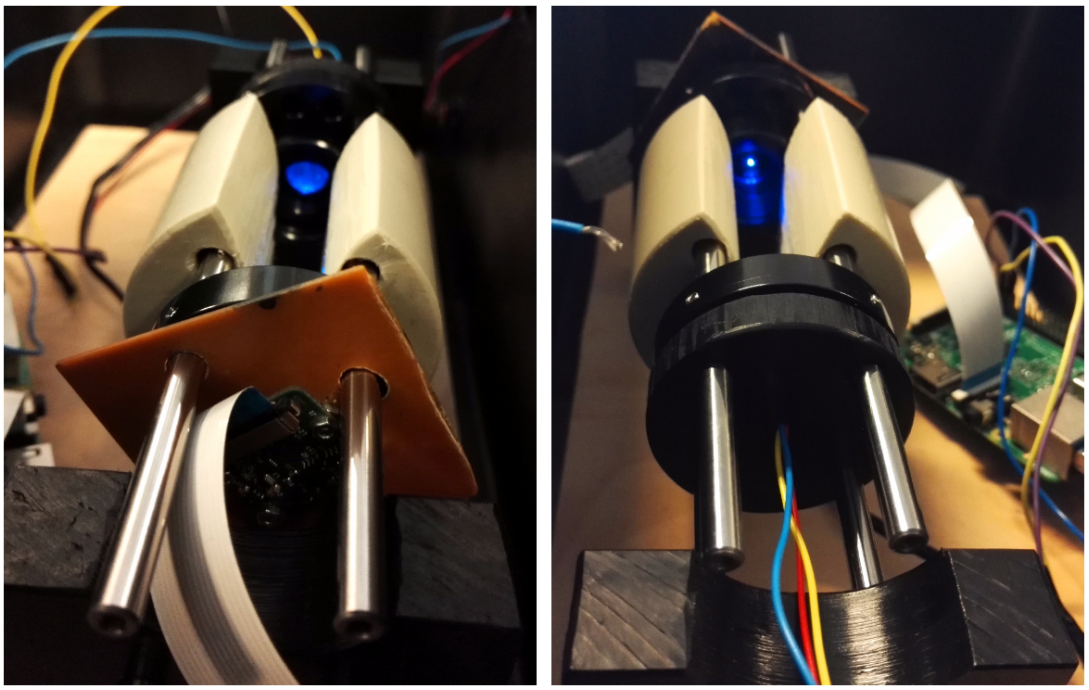

Figure 14: The measuring apparatus pictured from both ends. The picture on the left is the end where the camera module is placed and the picture on the right is the LED end.

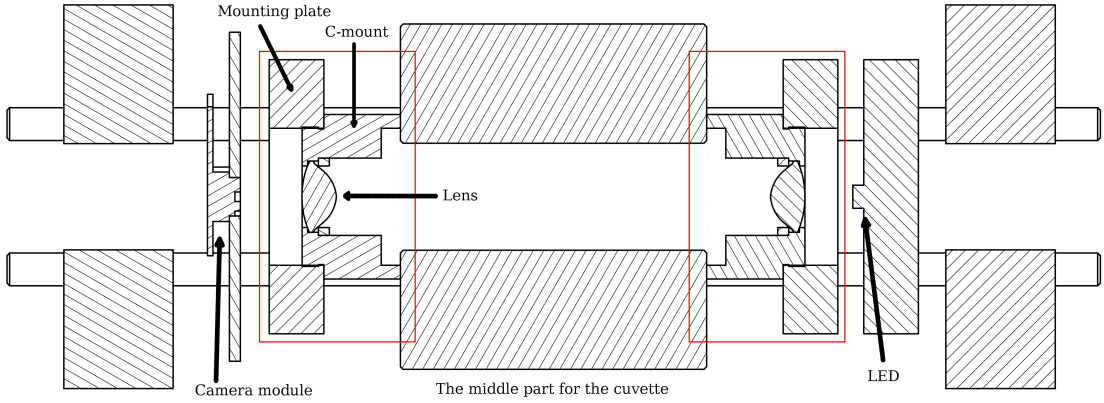

Figure 15: A schematic presentation of the light measuring apparatus, viewed from above. The camera sensor and the LED are positioned to both ends and between them is the lens system (circled in red) and the middle part for the cuvette.

presented in Figure 14. A more clearer view of the apparatus is presented in Figure 15 where the insides of the apparatus can be seen.

The LED and the camera module both are attached to in the middle of small plastic disks with double-sided tape. The disks can be placed to the supporting rods so that both components are also in line with everything else. The LED is part of a small electric circuit in which a transistor is used to turn the LED on and off. The circuit gets its input current from one the GPIO (General-purpose input/output) pins of the Raspberry Pi. These pins can be configured as both input or output and can be disabled or enabled from the Raspberry Pi. Thus the LED can be straightforwardly controlled from the computer. Like the LED, the camera module is also attached to the Raspberry Pi.

The LAB sample cuvette (HACH Lange 50 mm $\times$ 10 mm, product number LZM130) is placed between the LED and the camera module with another customized part. This cuvette model was chosen for the measurements because the same samples could be then measured also with a spectrophotometer. The middle part makes sure that the cuvette stays firmly in place during the measurements. This also allows the placement of the cuvette to the same position in every measurement. The light that the LED emits is collimated with two lenses. The lenses are placed inside small cylindrical C-mounts that are attached to the mounting plates.

The cage system is placed inside a black box to block light coming from the environment. An ethernet cable goes through a small drilled hole so that the Raspberry Pi can be accessed via a computer. The power cord of the Raspberry

Pi is also pulled through the hole. To prevent any light coming through the hole it is covered with black tape.

4.2 The components of the setup

As stated before, the data acquisition happens by taking pictures of the LED light source through the sample. To fully understand how the whole system works each part of the setup must be individually reviewed. This section concentrates on going through the steps how the light source is collimated to the camera sensor and how the camera sensor interprets the photons it receives.

4.2.1 Light source

A light-emitting diode (LED) serves as the light source in the apparatus. The advantages of LEDs include that they have good electronic modulation and they are small and low in cost. Nowadays there is a wide range of LEDs with different wavelengths available, ranging from ultraviolet region to near infrared. In addition, the lifetime of an LED is typically very long (40,000 – 50, 000 hours[3], depends on the temperature and humidity of the environment). For comparison lifetime of an incandescent light bulb is 750 – 20,000 hours[3]. However LEDs do not burn out like regular light bulbs and instead, their light output decreases over time.

In measurement applications, LEDs may be used as a replacement for more expensive parts such as UV-VIS laser diodes. Applications that take advantage of LEDs have been developed in the field of spectroscopy for example for the purpose of gas monitoring [36] and getting fluorescence information [37].

At first, the LED in usage was APA102c-LED [38] that is able to provide three different color outputs, blue, green, and red. However, it is possible to adjust the brightness of each color in the range of 0 to 255 and get a much larger number of color combinations. Although APA102c can produce many different wavelengths it was changed to a blue LED (product number KA-3528MBC) [39] because the blue LED has well-defined wavelength spectrum. The blue LED in question has the peak wavelength at 430 nm which corresponds the light emission of Bis-MSB.

[3]The hours refer to the concept of Average Rated Life (ARL) that means the time in which half of the lamps of the test sample have burned out [35].

The light output of the LED may vary over time, especially when the LED is turned on. It might take some time for the LED to emit light at full intensity. To make sure that the light output stays constant the intensity changes of the LED are also investigated in the measurements.

4.2.2 Light collimation

Light emitted by a point-like source spreads over a sphere as presented in Figure 16. Luminous flux from an LED spreads usually over a solid angle smaller than 180 degrees. Because of this a significant amount of light misses the sensor. Thus the light beam must be narrowed via collimator.

Though fully collimated (all light rays are parallel) light rays are not possible due to diffraction, light can be approximately collimated simply via a small hole. This kind of collimator narrows the beam sufficiently but also reduces luminous intensity of the beam because only a small portion of the light passes through the collimator. Instead of a hole collimator, light can be directed using an optical collimator.

Optical collimation is done with lenses. To execute successful measurements the lenses must be placed precisely to the system and their geometric properties must match with the system. The first lens collects the light emitted by the LED. LED emits light to some angle θ. To get the best performance out of the lens the acceptance angle of the lens should be equal or greater than θ. This ensures that most of the light is collimated. Figure 16 illustrates how the light is collimated to the sensor with two lenses.

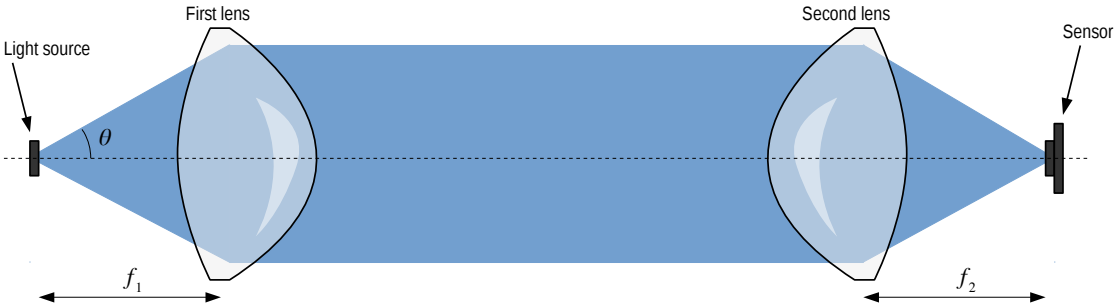

Figure 16: An illustration how the light emitted by the LED is collimated with lenses and focused on the (camera) sensor. The light cone that apex angle is denoted as θ must match the acceptance cone of the lens. The diameter of the lens and its focal length (f_1 and f_2 in the picture) define its acceptance cone. Reference is taken from [40].

The amount of light a lens can collect is stated with the f-number $f\#$, and the numerical aperture NA. These parameters are based on the focal length f, the diameter of the lens D, and index of refraction of the medium n. The f-number is the ratio between focal length and diameter [40]

$$f\# = \frac{f}{D}, \tag{15}$$

and the numerical aperture is defined as [40]

$$NA = \frac{1}{2 \cdot f\#} = n \sin\theta. \tag{16}$$

In our case, the viewing angle of the LED is informed to be 120 degrees [39]. This is the angle of the whole light cone, thus $\theta = 60^\circ$. The optical system is surrounded by air and therefore the index of refraction is chosen to be n = 1. With the given information the numerical aperture of the lens can be determined:

$$NA = n \sin\theta = \sin(60^\circ) = \frac{\sqrt{3}}{2} \approx 0.866025. \tag{17}$$

Calculating from the equation (15) the desired f-number $f\#$ for the lens is

$$f\# = \frac{1}{2 \cdot NA} = \frac{1}{2 \cdot \sqrt{3}/2} = \frac{1}{\sqrt{3}} \approx 0.577350. \tag{18}$$

The f-number now determines the size of the lens and what is the distance between the lens and the light source. For example, using a lens with f-number = 0.6 and D = 20 mm means that the focal length f of the lens is

$$f = D \cdot f\# = 20 \text{ mm} \cdot 0.6 = 12 \text{ mm}. \tag{19}$$

To match the light cone of the light source and the acceptance cone of the lens the light source must be placed to the focal point, that means at the distance of 12 mm from the lens. Note that this value varies from the real right placement for the lens. The LED is not a point-like light source and there are several optical aberrations like coma [41], spherical aberration [17], and chromatic aberration [17] that distort the light beam as it passes through the lens. The distance between the LED and the lens must be carefully tested to get the best possible outcome.

The lenses chosen for the setup were aspheric lenses with $D = 13$ mm and $NA = 0.88$ from Edmund Optics. These were the only available lenses with a numerical aperture higher than 0.866025. The lenses have a back focal length of 3.77 mm which means that the LED and the camera module must be placed approximately at this distance of off the backside of the lenses.

4.2.3 Camera as a light detector

CCDs (charge-coupled device) are widely used devices in digital imaging. They have many applications in natural sciences, for example in astronomy to get information about distant galaxies and in spectroscopy as the detector in optical spectrometers. Imaging sensors offer high quantum efficiency and their output is linear in contrast of input.

The Raspberry camera module in use has a Sony IMX219 8-megapixel CMOS sensor. CMOS sensors are more recent technology than CCD sensors. Compared to CCD sensors CMOS sensors are more inexpensive and easier to manufacture, and drain less power which extends battery life and decreases overheating problems [42]. For these reasons, CMOS are commonly used in devices like mobile phones and digital pocket cameras. The differences between these two technologies are irrelevant to this study since they register light in the same way [42].

A camera sensor is a solid-state device that collects the light. Upon hitting a pixel on the sensor the photons are converted to electrons. All photons are not converted to electron and every sensor has a different quantum efficiency (QE) which is the ratio of converted electron to incident photons. Pixels have a threshold how many electrons they can have: this threshold is called the saturation capacity. When exceeding the saturation capacity pixel cannot receive any more photons and the pixel appears as white in the picture. [43]

Since the pixel values of a photograph are related to the number of photons in particular pixel it is possible to use regular cameras as light meters. To use a commercial camera as a light meter the pixel values of the taken pictures need to be related to photometric quantities mentioned in Section 2.1.1. Pixel value N_d and luminance L_s have a relation in the form of [44]

$$N_d = K_c \left(\frac{tS}{f_s^2} \right) L_s, \tag{20}$$

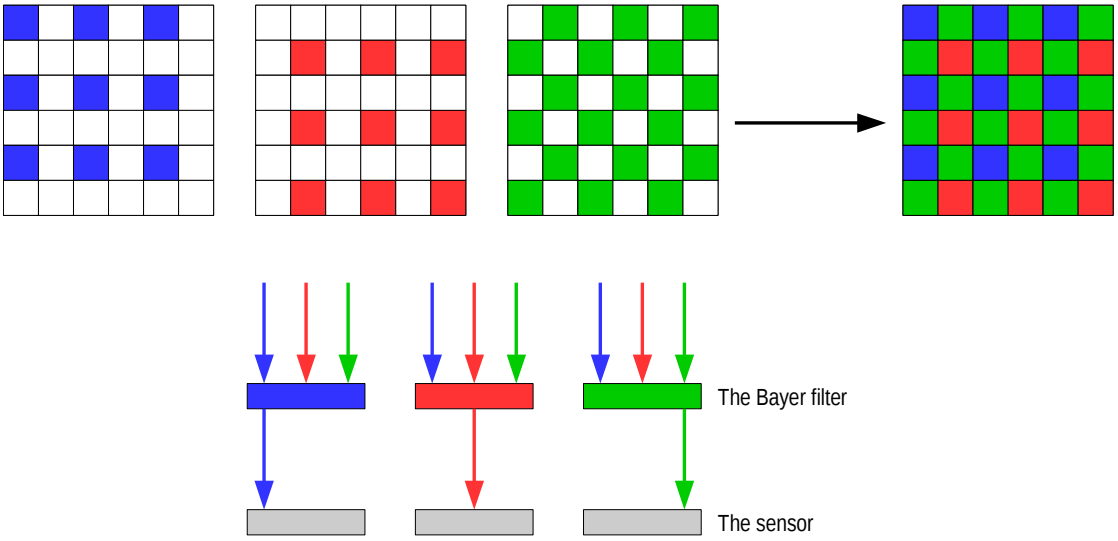

Figure 17: An illustration how the colors in the Bayer filter are arranged. The filter has red, green, and blue pixels that let photons in the respective wavelength range to pass to the pixel of the sensor. Reference is taken from [45].

where t is exposure time, f_s aperture number, S ISO value, and K_c the calibration constant for the camera. All these values except K_c can be determined from a picture taken with the camera and from its Exif data file. K_c is a constant that varies from camera to camera and can be found out taking pictures of a light source with known luminance L_s. For example, Hiscocks [44] demonstrates how K_c can be determined using the known luminance of the Moon. It might be possible to calibrate the camera using the blue LED that is part of the measurement setup, though the given values for the LED are not very precise. The datasheet of the LED notifies that the typical luminous intensity of the LED is 15 mcd. This means that luminance is 0.015 cd m^{-2}.

Even though the pixel value gives information about the light there are couple of matters affecting the output signal of the camera that needs to be taken account. Camera sensor gives a small signal even in circumstances in which light is excluded from the system. This so-called dark noise arises from the physical processes happening inside the sensor itself. The magnitude of dark noise is bound to temperature and thus the noise can be reduced lowering the temperature. Dark noise can cause problems in long exposure measurements such as imaging celestial bodies in astrophysics because the thermal electrons tend to pile up and cause the sensor to reach its saturation capacity faster. [43]

Another technical matter that has an effect on photon counting is related to the production of colored pictures. In photography, colored pictures are almost

always preferred over monochromatic ones that plain camera sensors produce. Colors for the pictures are produced attaching a color filter in front of the sensor. The most common color filter is the Bayer filter that has a color pattern seen in Figure 17. The principle of the Bayer filter is that the green squares let only photons of wavelength in the green region pass to the sensor, red squares let the red photons and blue squares the blue photons. This way three different color channels are created. Alone one channel produces a monochromatic picture but when these channels are combined the result is a colored picture. [42]

Bayer filter consists of 50 % of green pixels, 25 % blue pixels, and 25 % red pixel. As mentioned in Section 2.1, the human eye is most sensitive to green color and thus this is applied to the filter too. Bayer filter is quite a simple concept and does its job well in everyday photography but in low-light situations, it may lower the sensitivity: since one pixel in Bayer filter only passes a particular color out of three the flux of photons decreases by two thirds. [42]

Along with the noise signal and the Bayer filter processing, the image itself may include processes that modify the initial signal. The electronic signal produced by the camera sensor and the number of photons hitting the sensor have a linear relation. However, when the data is converted to an actual visible image format like JPEG the linearity is broken. JPEG pictures non-linearity is due to a process called gamma correction performed to pictures. Gamma correction is defined by [46]

$$V_{out} = V_{in}^{\gamma}, \tag{21}$$

where V_{out} is the gamma-corrected luminance that is the real value of luminance V_{in} raised to the power γ. Gamma correction is needed because the human eye does not perceive light in a similar fashion than a camera does. When there is an increase in brightness, human eye's response is logarithmic, not linear. Consequently, we are able to register small details and subtle changes in contrast [42].

The relation between the pixel values and light input is important to take into account. For example, the equation 20 requires that the pictures it is applied have a linear relation. The Raspberry Pi camera module, like many other cameras, are capable to capture the raw data. These raw files have a linear relationship with light input the sensor receives unlike compressed formats like JPEG. Still, the usage of raw image format is tedious, especially with Raspberry Pi. Raw images have sizes in order of megabytes, which means hundreds of times bigger than simple JPEG images of the size of kilobytes. Since the number of images taken with Raspberry Pi can exceed 100 hundred pictures in one measurement it runs quickly out of space if the raw format is used. In addition,

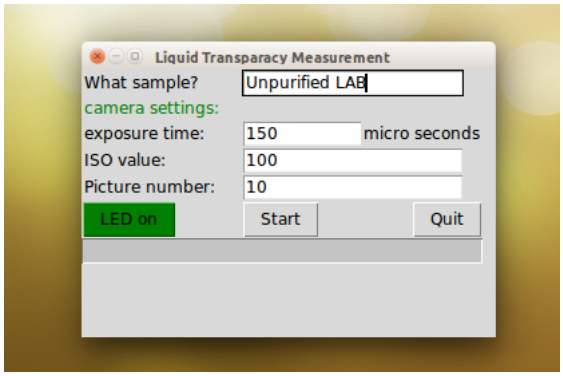

Figure 18: The user interface of the program for the apparatus. The number of pictures to be taken can be adjusted, as well as info about the sample. The camera settings include setting ISO value and exposure time. Setting a right exposure time is especially important so that the images do not get oversaturated.

moving the pictures from Raspberry Pi to another computer can take a lot of time if using raw format.

4.3 Software

Software for Raspberry Pi has been written in Python 2.7. Python was chosen for the programming language because it is fully compatible with Raspberry Pi, easy to write and read, and it has several useful modules to be utilized in this study. For example, the camera module can be controlled via Python's picamera-module, and the final analysis is also done inside the Python-code.

The graphical user interface of the program can be seen in Figure 18. Various setting regarding the LED and the camera module can be found at the interface. Exposure speed in microseconds and ISO-value can be set for the camera module. Info about the sample used in the measurement can be written to the 'What sample?'-entry while a number of pictures can be given to 'Picture number'-entry.

The measuring process starts by pressing 'LED on'-button. The measurement can be started by pressing 'Start'-button after all the settings for the camera module are set. The camera module takes set number of photographs and saves the photographs to a measurement directory the program creates. Then a Gaussian fit is performed to the pictures with a separate Python code so that further analysis can be made.

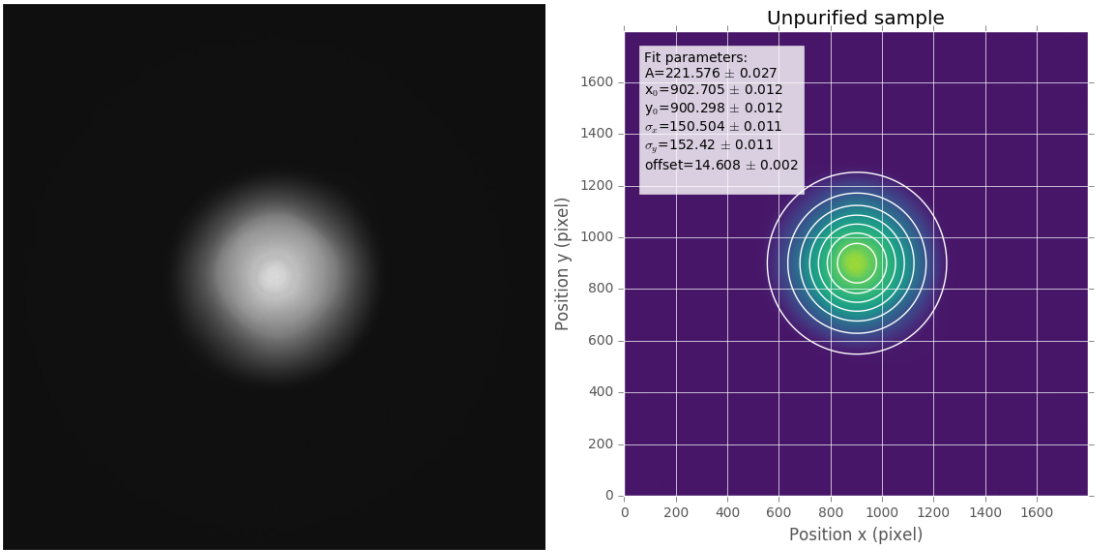

Figure 19: An example output of one measurement where unpurified LAB sample was analyzed by taking 100 images. The left image shows the grayscale image containing mean values of the 100 images; the right image shows the Gaussian fit to the latter, having also all the parameters listed.

The pictures have a resolution of 2592×1944. In order to perform the Gaussian fit arrays with matching dimensions (1800×1800) are constructed on the pictures. The pictures are first converted to grayscale. Grayscale images contain only information of the intensity of the light in the range of 0 to 255 and this is the only relevant information we need from the pictures. The size of the arrays is based on the center of the LED i.e. the brightest spot in the pictures which was determined to be $(996, 1231)$. This is a fixed value and should be the same in every measurement since the camera and LED stay in place. It must be specified again if modifications are made to the hardware.

The arrays are summed up in a loop and then divided by the number of arrays (same as the number of pictures). This way we get one array containing the mean pixel values of all the pictures taken in the measurement. An error array is also calculated and it contains standard error for every pixel value in the mean value array.

Since the light source has a profile that resembles Gaussian function a two-dimensional Gaussian function is fitted to the data in the mean value array. The two-dimensional Gaussian function is

$$f(x,y) = z_0 + A \exp\left(-\frac{(x-x_0)^2}{2\sigma_x^2} + \frac{(y-y_0)^2}{2\sigma_y^2}\right), \tag{22}$$

where z_0 is the offset, A is the amplitude of the light source, (x_0, y_0) is the center, and σ_x and σ_y are standard deviations of x and y respectively. Figure 19 shows a picture of the LED accompanied by a graph with the fit. This approach makes it possible to compare the changes in the peak intensity and the variation of the light when measuring different samples.

5 Measurements

Measurements utilizing the custom-made experimental setup described in Section 4 were performed to study the light attenuation in LAB samples before and after their purification process. In addition, spectrophotometry measurements were done to use as a comparison to the results of the Raspberry Pi setup. The measurements were carried out in the chemistry laboratory of Pyhäsalmi Mine, and with two different samples: with a LAB sample from Russia (manufacturer being Kirishi) and with another from China (named Jingtung special LAB 201506, from JUNO experiment). Another sample from Daya Bay was used as a reference sample. The Daya Bay sample has gone through all three different purification methods mentioned in Section 2.2.3. Small portions of PPO (3 $\mathrm{g\,l^{-1}}$) and Bis-MSB (15 $\mathrm{mg\,l^{-1}}$) have been mixed to the Daya Bay sample [7].

The purification method for Russian and Chinese samples is column chromatography. The whole sample apart from a small sample referred as the raw sample onwards is poured to the column and let go through it. The process is quite slow and therefore the change to the next sample is performed usually the day after. The next step is to salvage a small portion once purified sample and pour the sample again into the column. This action is repeated as many times as

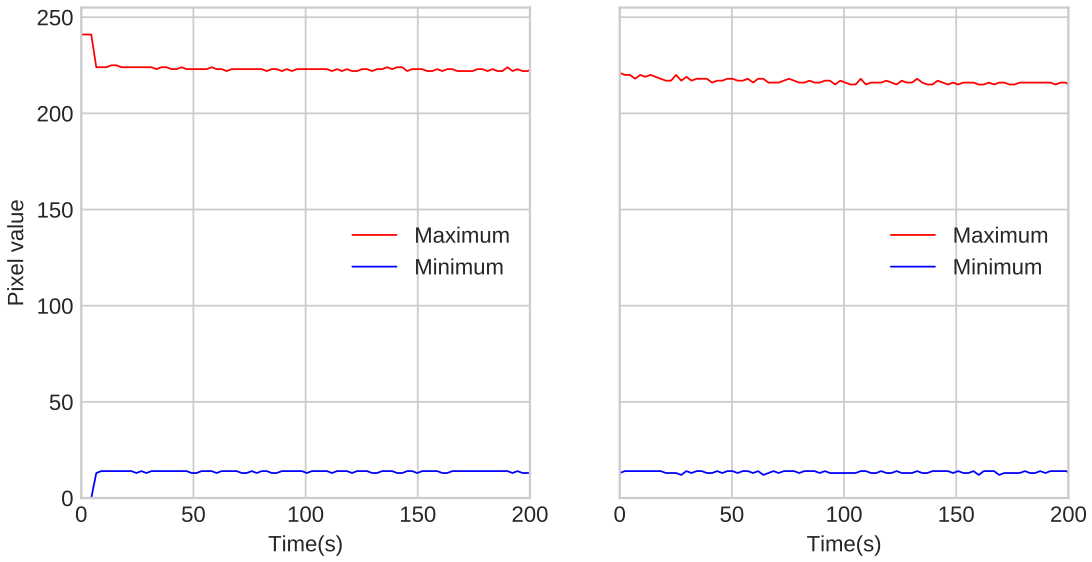

Figure 20: Graph representing the maximum pixel value (red) and the minimum pixel value (blue) of a picture taken of the LED as the function of time. A small jump around 8 seconds can be seen in the measurement from the first measurement session (left graph). The jump vanishes when a 10 second waiting period is added to the code (right graph).

there is sample left. After the purification process, we have different samples that have been purified different times and these samples are measured with both spectrophotometer and the Raspberry Pi setup.

As stated before in Section 4.2.1 the light output of the LED may differ in time. Figure 20 shows maximum and minimum pixel values of pictures taken in a measurement as a function of time. The first graph corresponds the measurement with unpurified Russian LAB sample and the second one corresponds unpurified Chinese sample. A small jump in both the maximum and the minimum can be seen around 8 seconds but then the values stay quite constant. The time cap is rather long and might result from the electrical circuit the LED is part of. However, the small jump can be rejected adding a waiting period of ten seconds to the code after switching the LED on. The 10 seconds waiting period was implemented to the measurements with the Chinese samples and as seen in the graph the values stay on the same level.

5.1 Test measurements with the Russian LAB sample

The measurements on the Russian sample were performed to raw sample and one to four times purified samples. Daya Bay sample was measured three times. The spectrophotometer was calibrated using one empty cuvette but had to be calibrated again using possibly different one: the lack of adequate amount of LAB under a couple of samples meant that more LAB had to be filtered. These samples had to be measured the next day and the spectrophotometer had to be calibrated again. This might have caused some error between the samples measured different days since the cuvettes showed some difference between each other when checked with the spectrophotometer.

The calibration of the spectrophotometer (Hach Lange, DR 2800) is done with a 50 mm long PMMA cuvette, compatible with the spectrophotometer. The spectrophotometer states transmittance through the sample and also absorbance. After the calibration, the cuvette is filled with a sample, measured with the spectrophotometer, and measured with the Raspberry Pi system. The same sample is then bubbled with nitrogen gas (99.999% pure nitrogen) to remove oxygen from the samples. The same measurement procedure is repeated with the bubbled sample.

This measurement served more as a test for the Raspberry Pi setup and the whole sample purification/preparation process. The results do not tell much about the effectiveness of the purification, as can be seen from Figure 21. How-

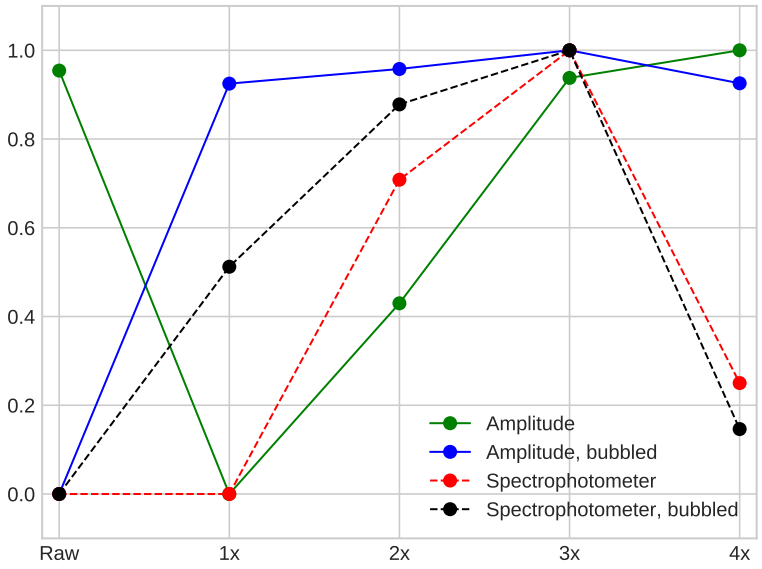

Figure 21: Comparison between the relative values of amplitudes of the LED light and the relative transmittances measured with the spectrophotometer. This data is from the first measurement with the Russian LAB sample. As we can see the values do not increase the more the sample is purified in all of the cases but are quite random.

ever, the measurement gave us insights what can be done differently and better in the next measurement session.

5.2 Measurements with the Chinese LAB sample

These measurements started in the same manner as the previous test measurements with the Russian LAB samples. The Chinese sample was purified three times resulting four different samples. This time degasification was performed in an enclosed spaced filled with nitrogen gas that is the glove bag seen in Figure 22. The pyramid-shaped bag has external dimensions of $860 \times 560 \times 725$ mm (L×W×H) and it has a small gas insertion valve on the backside. An oxygen meter was used to ensure that oxygen levels remained safe at the working station during the whole measurement procedure. The glove bag seemed airtight since the oxygen percentage remained the same.

The measurement procedure differed a bit compared to the first measurements since the degasification was performed in the glove bag. First, the spectrophotometer was reset with an empty PMMA cuvette and then the first, unpurified sample was measured with both spectrophotometer and the Raspberry Pi setup. Then the spectrophotometer was reset again with another empty cuvette. This

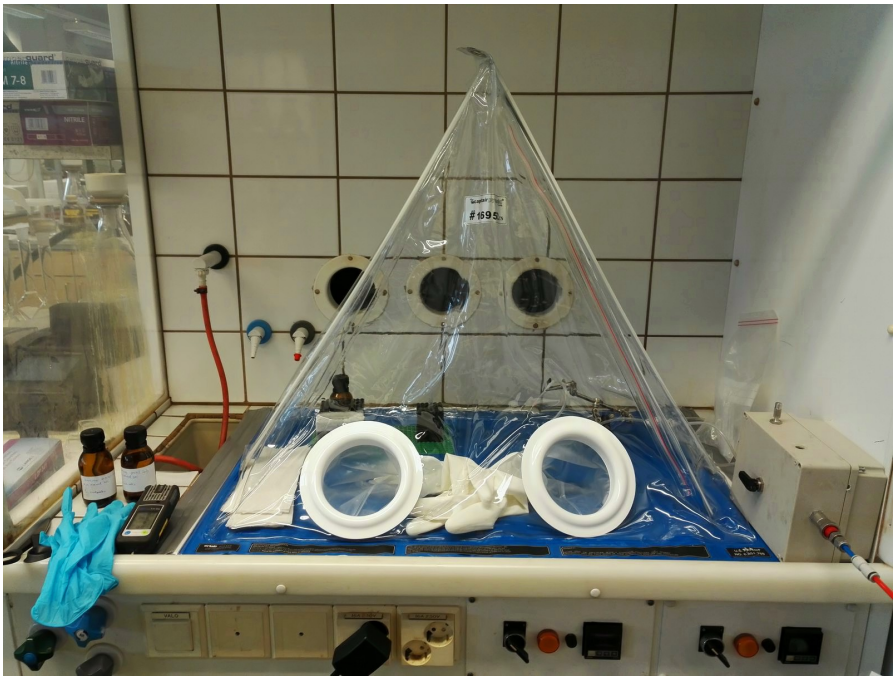

Figure 22: Picture of the working station where LAB samples were prepared. The pyramid in the middle was filled with nitrogen (the nitrogen is located on the right side, outside the picture). On the left of the pyramid, a pair of nitrile gloves, an oxygen meter, and a couple of LAB sample bottles can be seen.

time the cuvette and a sample bottle containing the unpurified sample were put in the glove bag. The sample, still inside the bottle, was bubbled with nitrogen for more than 5 minutes and then moved to the cuvette using a pipette. After closing the cuvette with a lid it was removed from the glove bag and measured in the same manner as the previous sample.

These measurements were carried out with much more precision than the previous ones. Performing degasification in the bottles rather than in the cuvettes and then using a pipette to fill the cuvettes prevented spilling LAB and contaminating the cuvettes. However, maintaining an oxygenless environment turned out to be difficult since the measuring equipment did not fit into the glove bag and it needed to be open every time a bubbled sample was to be measured. At the end of the measurement session, the oxygen percentage was measured as 10 % in the glove bag after opening it.

5.3 Sources of uncertainties

Since we are measuring quantities that deviate very slightly, addressing the sources of uncertainty in a measurement is in place. The first source of error is the electronics. Even if everything is steadily inside the system and several pictures are taken, they still differ from each other. This is due to the dark noise in the camera sensor discussed in Section 4.2.3 and the varying light output of the LED, or so-called shot noise [43]. In any case, taking a large amount of pictures results in a smaller standard error and thus the estimate is better.

A more difficult error source to handle is the error arising from the placement of the cuvette. The cuvette needs to be moved between the measurements and this may affect the results when comparing two different measurements. The cuvette fits quite firmly to the middle part of the setup but yet it has some leeway. To examine the deviation in different measurements a cuvette filled with water was measured 100 times while removing and replacing it back to the setup between the measurements. Figure 23 shows a histogram filled with the mean pixel values determined from each measurement. As can be noticed, the mean

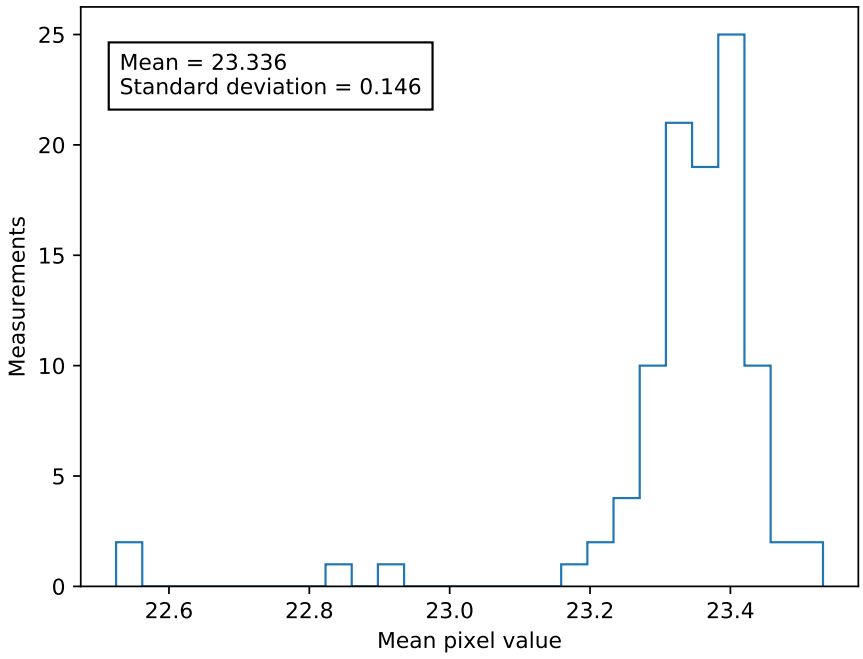

Figure 23: A figure showing the deviation in cuvette placement. The mean pixel values from the measurements are mostly located near the mean 23.336, having a couple of measurements scattered to lower values.

values of different measurements with the same sample can deviate quite much compared to the difference we actually need to measure.

6 Simulations

Testing the experimental setup by measuring LAB samples is needed to understand the whole procedure. However, it proved difficult to judge the functionality of the setup based only on the measurements since the results were not precise enough. Simulating the setup makes it possible to inspect what kind of results are to be expected from the setup with different parameters. In this case, these parameters include attenuation length of the sample and the path length of the cuvette. The purpose of the simulations is to estimate the accuracy of the current setup and to find out if the setup could be improved.

Geant4 [47] is an object-oriented toolkit for creating physics simulations in various fields such as heavy-ion physics, astrophysics, and medical physics. The toolkit is written in the C++ language and is maintained by CERN. To create a simple simulation three mandatory classes included in the Geant4 package are needed: G4VUserDetectorConstruction for defining geometry for the detector or setup, G4VUserPhysicsList for the physical processes that can happen in the system, and G4VUserActionInitialization in which user needs to initialize at least a user action class called G4VUserPrimaryGeneratorAction. This class initializes the particle source for the simulations. Figure 24 shows the structure of the simulation program used in this study.

The simulation process is simple: a chosen number of photons is shot through the LAB sample towards a sensitive detector that imitates the camera sensor. Upon hitting the sensitive detector the hit is counted and after the run, the sum of all registered hits is received. The simulation is repeated with several dif-

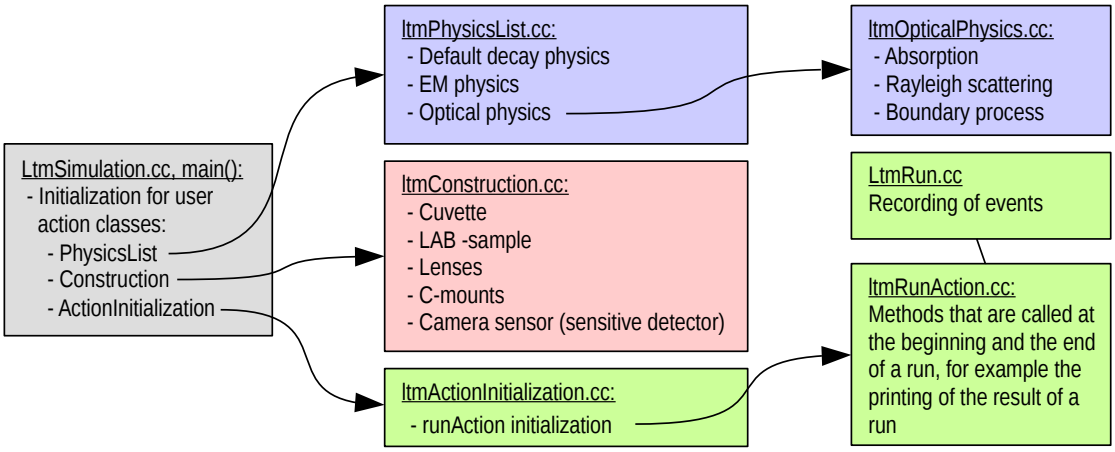

Figure 24: Chart that shows the classes used in the simulation and the main components they include.

ferent attenuation lengths to find out how much difference samples varying in their purity are expected to have. Different components of LAB have been taken into account: the abundances of each LAB component used in the simulations can be found from the reference [24]. Construction contains also the PMMA cuvette for LAB, and the lenses and the C-mounts from the real-life setup.

The lenses are constructed from one cylindrical part and two sections of ellipsoids attached to both sides of the cylinder. All the necessary parameters for the lens construction can be derived from the 3D model provided by Edmund Optics. As mentioned in Section 4 the lenses are aspheric from the other side but for simplicity, both sides of the lens are spherical in the simulations. This choice should not have a notable effect on the results because the aspheric lens only focuses light better compared to a spherical lens. The real lenses are made of optical glass and the material is composed of several different compounds.

To simulate the behavior of light a particle source shooting opticalphotons, that is Geant4's own glass, is defined using GeneralParticleSource-class. This class enables various options for the light source, for example, defining the geometry of the source, the position, distribution, and the energy spectrum. The

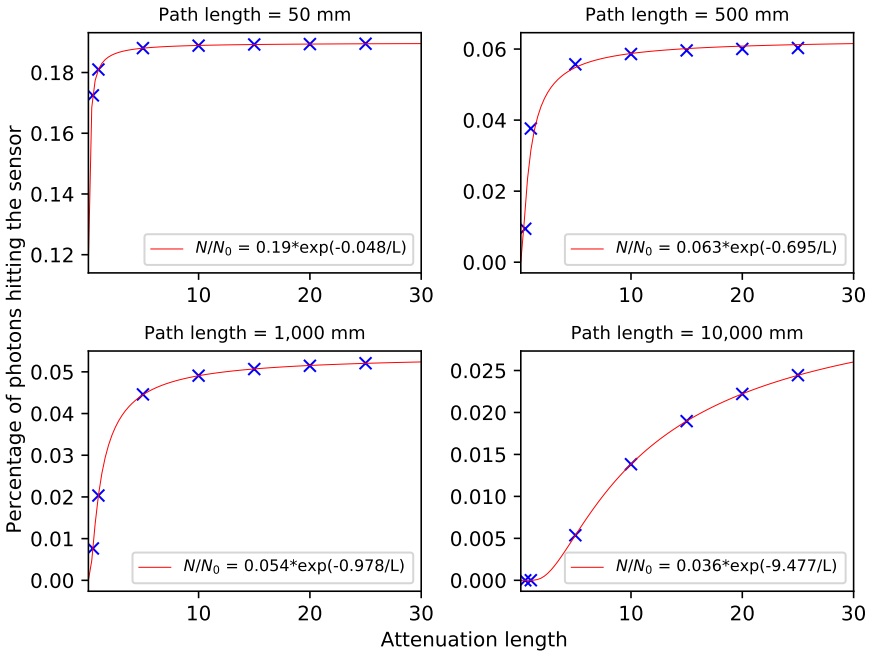

Figure 25: Simulations for cuvettes with different path lengths. The ratio of photons that hit the sensor to all shot photons was calculated using different attenuation lengths for the samples. The y-axis tells the ratio whereas the attenuation length is on the x-axis. The curves follow the light attenuation equation derived from Beer-Lambert law.

photon source is placed to the focal point of the lens and its energy distribution corresponds the distribution of the LED as well as possible. Physical processes needed for the simulations include implementation of absorption, Rayleigh Scattering, Mie Scattering, and boundary processes happening between two interfaces.

Figure 25 shows how many photons N out of generated photons $N_0 = 2 \times 10^7$ hit the sensor at different attenuation lengths of LAB. The simulation is also run with different path lengths: cuvette is stretched from 50 mm to 500 mm, 1,000 mm, and 10,000 mm. The simulations give an insight what precision the setup has to exceed to give meaningful information about the optical purity of the samples.

Simulations were also performed with an empty cuvette and without any cuvette. Using a 50 mm path length gives out $N/N_0 = 0.148774$ and $N/N_0 = 0.172389$ respectively. The ratio is less through air than through LAB that has $N/N_0 = 0.188038$ when $L = 5$ m. As stated in Section 2.1.2, this is due to reflections and refractions in different interfaces. The ratio is also lower than simulation including LAB in the situation in which there is no cuvette. In the situation where there is a cuvette filled with a sample, the photons stay inside the cuvette because of internal reflections. These photons are likely to reach the camera sensor. When there is no cuvette these photons escape the system and thus are not registered by the sensor. Figure 26 shows the geometry used in the simulations and the distribution of photons in both LAB and air situations.

Equation (9) can be represented by the number of photons instead of intensity since intensity is proportional to the number of photons. Thus Equation (9) can

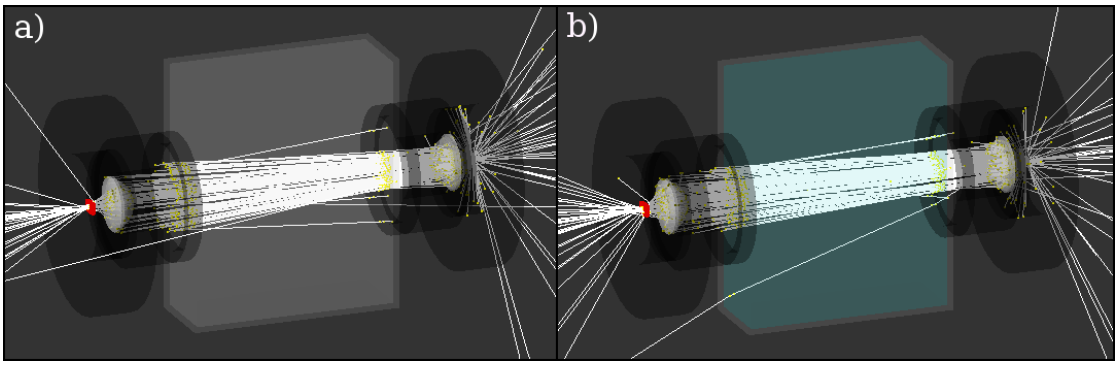

Figure 26: Picture representing the simulation geometry and how the photons propagate the system. Picture a) simulates the situation where there is no sample in the cuvette, and in Picture b) LAB is present. Close examination of the two images shows the effect of refraction: light rays in Picture a) are refracted slightly more than in Picture b) and therefore fewer photons reach the camera sensor (the red part).

Table 2: Values of L_2 estimated with simulation results. The resolutions listed correspond different image formats that can be taken via Raspberry Pi camera module.

Resolution	$x = 50$ mm	$x = 500$ mm	$x = 1,000$ mm	$x = 10,000$ mm
8-bit	$<$ 2.06552 m	$<$ 7.29197 m	$<$ 8.19935 m	$<$ 17.0386 m
10-bit	$<$ 6.65998 m	$<$ 15.7044 m	$<$ 16.6993 m	$<$ 22.537 m
24-bit	$<$ 24.9959 m	$<$ 24.9991 m	$<$ 24.993 m	$<$ 24.9998 m

be fitted to the data. The fit results can be seen in Figure 25. As we can see, the attenuation in the setup follows the theory quite closely. There is a coefficient that needs to be added in order that data fits the exponential function. The coefficient is related to the other sources of the light attenuation besides LAB itself.

With these fit curves, it is possible to estimate the resolution of the experimental setup. The current setup takes pictures that can have 256 different colors; this means that the setup can ideally distinguish differences that are larger than 0.4 %. Let us examine two samples: an unpurified sample and a purified sample with attenuation lengths of L_1 and L_2 respectively. Let's assume that $L_2 = 25$ m, a value mentioned in Section 2.1.2. It can then be estimated how unclean the unpurified sample has to be in order to distinguish it from the purified sample using the current setup. The difference between light yields has to be larger than 0.4 % i.e.

$$P(L_2) - P(L_1) = \left(\frac{N}{N_0}\right)_2 - \left(\frac{N}{N_0}\right)_1 > 0.004.$$

Using result from the simulation with 50 mm cuvette $P(L_1)$ and $P(L_2)$ can be written as

$$0.19 \cdot (\exp(-0.048/25) - \exp(-0.048/L_2)) > 0.004$$

This inequality gives an upper limit of 2.06552 m to L_2. If the unpurified sample has an attenuation length larger than that it cannot be distinguished from the purified sample. It is also good to keep in mind that this is the ideal situation: the real attenuation length most certainly will be smaller than this. However, the unpurified sample has to be ever so unclean so that the setup can be used with its existing capabilities.

A similar comparison can be performed also to the other cuvette lengths. The upper limits of L_2 for every simulated cuvette length are presented in Table 2.

The limits are also calculated using different bit depths for images: 10-bit and 24-bit. It has been informed in Chapter 5 of Raspberry Pi documentation [48] that raw bayer data taken by the Raspberry camera module consists of 10-bit values. In addition, Raspberry Pi camera module is capable of taking images in which the green, blue, and red data are saved to three different 8-bit channels. Combining the color channels results in a 24-bit RGB data array which corresponds to 16,777,216 different colors. Using 10-bit images means that a change of 0.1 % could theoretically be detected. Correspondingly, 24-bit images mean a change of $6 \cdot 10^{-6}$ %. According to the values of L_2 in Table 2, the performance of the setup could be improved a lot by changing the image format.

7 Results

The results from the spectrometer are presented in Table 3 and Table 4. The absorbance values are negative since the samples were compared to empty cuvettes and the intensity through an empty cuvette is smaller than through a filled cuvette as explained in Section 2.1.2. Considering the values in Table 3 the results seem very random and do not have any order. Values of Daya Bay sample also vary as much as all the other samples which means that the system was not stable enough to distinguish the Russian samples. These results arise most likely from contamination caused by LAB itself. In addition, the cuvettes used in this measurement session were not unused and therefore all of them might not have been in the same condition.

The values in Table 4 are related to the second measurement session in which the glove bag was utilized and cuvettes were unused. Like in previous measurements, no conclusions can be made about the impact of purification times and removal of oxygen since the values are almost the same. However, the values are less deviated compared to the values in Table 3 which means that if the spectrophotometer cannot see any difference between the samples the measurement procedure itself was improved compared to the procedure when using the Russian LAB.

The measurements with the Raspberry Pi setup did not perform any better: the differences between samples were as large as the differences between the mea-

Table 3: Results of spectrophotometer measurements with Russian LAB. This is the first measurement session out of the two. The results did not have any consistency which may result from contamination in cuvettes. Based on these measurements another session with better LAB handling was carried out.

LAB sample	Non-bubbled		Bubbled	
	Absorbance	Transmittance (%)	Absorbance	Transmittance (%)
Unpurified	-0.019	104.6	-0.014	103.3
1x purified	-0.020	104.6	-0.023	105.4
2x purified	-0.027	106.3	-0.029	106.9
3x purified	-0.029	107.0	-0.031	107.4
4x purified	-0.022	105.2	-0.017	103.9
Daya Bay 1	-0.016	103.7	–	–
Daya Bay 2	-0.014	103.2	–	–
Daya Bay 3	-0.025	105.8	–	–

Table 4: Results of spectrophotometer measurements with Chinese LAB. This is the second measurement session. Anything about the purity order cannot be concluded from these measurements either but the results seem to be less deviated than in the first measurement session.

LAB sample	Non-bubbled		Bubbled	
	Absorbance	Transmittance (%)	Absorbance	Transmittance (%)
Unpurified	-0.024	105.7	-0.025	105.9
1x purified	-0.020	104.7	-0.024	105.8
2x purified	-0.022	105.3	-0.022	105.1
3x purified	-0.024	105.7	-0.024	105.6
Daya Bay 1	-0.023	105.4	–	–
Daya Bay 2	-0.026	106.1	–	–
Daya Bay 3	-0.032	107.7	–	–
Daya Bay 4	-0.023	105.5	–	–

surements with the reference sample. In light of the reference sample measurements, it seems that the differences are caused by some interference rather than by the attenuation in the sample. The displacement of the cuvette between the measurements discussed in Section 5.3 may be the biggest reason why there is any deviation between the samples. According to the simulations reviewed in Section 6, the current setup should not see any difference between the samples assuming that the unpurified samples had attenuation length longer than 2 m.

Other matter worth of mentioning is the fact that even if the cuvette had a path length of $10,000$ mm it still wouldn't be enough with the current setup. The difference in the attenuation length between the unpurified and the purified sample would still need to be approximately at least 8 m if the purification had yielded a sample with attenuation length longer than 25 m. The path length needs to be drastically longer than 10 meters to get reasonable results out of the current setup. However, as the L_2 values for 24-bit images in Table 2 show, the performance can be improved from the software side. This again requires that a better solution is found for the middle part of the setup since the error in the cuvette placement must be minimized as much as possible.

8 Summary and discussion

This study's main purpose was to find out if LAB samples with high attenuation lengths and different purities could be distinguished from each other with the built experimental setup described in Section 4. The study included measurements done with the setup as well as simulations. Unfortunately, this could not be done with the current setup. The reasons why this is the case originated from the inadequate path length of light and dynamic range of the JPEG pictures. The cuvettes used as the containers for LAB had only a path length of 50 mm. For samples that are not optically very clear, this might do well enough but LAB can have attenuation length higher than 20 m. This means difference less than half a percent when using cuvette with this short path length. Our setup utilizes 8bit JPEG pictures which means that the pixel scale is from 0 to 255. One step is then approximately 0.4 % whereupon hypothetically the setup could spot the difference between samples that have attenuation difference greater than 0.4 %. This does not count in the error arising from the displacement of the container which adds to the percentage.

The dynamic range of pixel can be raised using other formats: JPEG was first chosen since it did not need much post-processing and the JPEG pictures are small sized. Raspberry Pi camera module supports 24bit RGB format that could be used to get more precise information. In Section 6 the simulations suggest that changing the format could improve the setup even if the sample vessel is not very long. Changing the image format requires that the data saving is done sensible way since the RGB data files are big. However, the increase in precision of the images is meaningless if errors caused by displacement of the container are the same scale as in the measurements mentioned in Section 5.

Besides the image format, the gamma correction mentioned in Section 4.2.3 must be taken into account in future if the camera module is in use. Another modification that is related more to the light source is to add an additional optical filter to the system. Although the blue LED is informed to have wavelength peak of 430 nm it still emits quite a wide range of photons with different wavelengths. The optical filter would ensure narrower wavelength range if the measurements require a better understanding of the energy spectrum of the photons.

As for the sample cuvettes, the 50 mm cuvettes must be replaced for the sake of better results. These small cuvettes worked well in the testing of the apparatus but are not a very good long-term solution. Even though LAB doesn't react with acrylic, the cuvette lids do. The acrylic cuvettes also cannot be cleaned for the purpose of reuse: acrylic does not withstand alcohols and it is very challenging

to get rid of LAB using ordinary detergents. Therefore a glass product might be the best solution for a reusable sample vessel.

The cost of the current setup is approximately 270 euros, not including the cuvettes and the middle part for the cuvettes. Components used for data acquisition cost only around 46 euros but the rigid structure ended up cost 210 euros. The overall price is reasonable compared to other setups focusing on same subjects which have sample containers with much greater volumes and PMT used for DAQ. With the right corrections, the setup could be used in smaller scale liquid scintillator transparency analyses.

References

[1] W.R. Leo. *Techniques for Nuclear and Particle Physics Experiments: A How-to Approach*. Springer, 1987.

[2] T. Lassere et al. SNIF: A Futuristic Neutrino Probe for Undeclared Nuclear Fission Reactors. *Physical Review C*, 2010. arXiv:1011.3850.

[3] P. Vogel, J. F. Beacom. Angular distribution of neutron inverse beta decay, $\bar{\nu}_e + p \rightarrow e^+ + n$. *Physical Review D*, 60, 1999. arXiv:hep-ph/9903554.

[4] C. Giunti, C. W. Kim. *Fundamentals of Neutrino Physics and Astrophysics*. OUP Oxford, 2007.

[5] O. Yu. Smirnov et al. Measurement of neutrino flux from the primary proton-proton fusion process in the Sun with Borexino detector. 2015. arXiv:1507.02432.

[6] M. Chen. The SNO+ Experiment. 2008. arXiv:0810.3694.

[7] Z. Djurcic et al. JUNO Conceptual Design Report. 2015. arXiv:1508.07166v2.

[8] T. Enqvist et al. Measuring the ^{14}C content in liquid scintillators. *Journal of Physics: Conference Series*, 718, 2016. DOI:10.1088/1742-6596/718/6/062018.

[9] Callio Lab, Underground center for Science and R & D, webpage. `http://calliolab.com`. Accessed 8.12.2017.

[10] G. Alimonti et al. Measurement of the ^{14}C abundance in a low-background liquid scintillator. *Physics Letters B*, 422(1-4):349–358, 1998.

[11] Xiao Hua-Lin, Deng Jin-Shan. Oxygen quenching in LAB based liquid scintillator and nitrogen bubbling model. 2009. arXiv:0904.1329v4.

[12] R. McCluney. *Introduction to radiometry and photometry, 2nd edition*. Artech House, Boston, 2014.

[13] M. Kalloniatis, C. Luu. Psychophysics of Visions. `http://webvision.med.utah.edu/book/part-viii-gabac-receptors/psychophysics-of-vision/`. Accessed 8.12.2017.

[14] DIAL company. Efficiency of LEDs: The highest luminous efficacy of a white LED. `https://www.dial.de/en/blog/article/efficiency-of-ledsthe-highest-luminous-efficacy-of-a-white-led/`. Accessed 8.12.2017, 2016.

[15] Thorlabs: Optical substrates. `https://www.thorlabs.com/newgrouppage9.cfm?objectgroup_id=6973`. Accessed 8.12.2017.

[16] Lars Øgendal. Light Scattering: a brief introduction. 2016. Available on http://www.nbi.dk/~ogendal/personal/lho/LS_brief_intro.pdf. Accessed 8.12.2017.

[17] Randall Knight. *Physics for Scientists and Engineers: A Strategic Approach with Modern Physics*. Pearson, 3 edition, 2013.

[18] P. Pfahler. Basic mixing and purification of liquid scintillators. *Angra Neutrino Project notes*. Available on http://lsd.cbpf.br/neutrinos/pages/documents.php. Accessed 8.12.2017.

[19] B. Valeur, M. Berberan-Santos. *Molecular Fluorescence: principles and applications*. Wiley, 2 edition, 2013.

[20] J. Goett et al. Optical attenuation measurements in metal-loaded liquid scintillators with a long-pathlength photometer. *Nuclear Instruments and Methods in Physics Research A*, 637(1):47–52, 2011.

[21] H. Yang et al. Light Attenuation Length of High Quality Linear Alkyl Benzene as Liquid Scintillator Solvent for the JUNO Experiment. 2017. arXiv:1703.01867.

[22] X. Zhou et al. Rayleigh scattering of linear alkylbenzene in large liquid scintillator detectors. *Review of Scientific Instruments*, 86, 2015. DOI:10.1063/1.4927458.

[23] I.S. Yeo et al. Measurement of the refractive index of the LAB-based liquid scintillator and acrylic at RENO. *Physical Scripta*, 82(6), 2010. DOI:10.1088/0031-8949/82/06/065706.

[24] I.B. Nemchenok et al. Liquid Scintillator Based on Linear AlkylBenzene. *Physics of Particles and Nuclei Letters*, 8(2):129–135, 2011.

[25] Linear alkylbenzene material safety data sheet (MSDS). http://www.uolab.lsu.edu/documents/MSDS/Linear_Alkylbenzene.pdf. Accessed 8.12.2017.

[26] P. Huang, P. Li, Z. Fu, C. He, Y. Ding, J. Li, M. Qi. Study of attenuation length of linear alkyl benzene as LS solvent, 2010.

[27] K. D. Neame, C. A. Homewood. *Introduction to liquid scintillation counting*. London Butterworths, 1974.

[28] M. Yeh, A. Garnov, R. L. Hahn. Gadolinium-loaded liquid scintillator for high-precision measurements of antineutrino oscillations and the mixing angle, θ_{13}. 578:329–339, 2007. DOI:10.1016/j.nima.2007.03.029.

[29] J. K. Ahn et al. RENO: An Experiment for Neutrino Oscillation Parameter θ_{13} Using Reactor Neutrinos at Yonggwang. 2007. arXiv:1003.1391.

[30] M. Apollonio et al. Limits on Neutrino Oscillations from the CHOOZ Experiment. 1999. arXiv:hep-ex/9907037.

[31] M. Goodman, T. Lasserre. Double Chooz, A Search for the Neutrino Mixing Angle θ_{13}. 2016. arXiv:hep-ex/0606025.

[32] P. Kuusiniemi et al. Underground cosmic-ray experiment EMMA. *Journal of Physics: Conference Series*, 409, 2013. DOI:10.1088/1742-6596/409/1/012067.

[33] J. Joutsenvaara. Deeper understanding at Lab 2: the new experimental all at Callio Lab underground centre for science and R & D in the Pyhäsalmi Mine, Finland. 2016.

[34] G. Bonvicini, N. Harris, V. Paolone. The chemical history of ^{14}C in deep oilfields. 2003. arXiv:hep-ex/0308025.

[35] What Does Average Rated Life Mean? `http://www.bulbs.com/learning/arl.aspx`. Accessed 8.12.2017.

[36] M. Degner, H. Ewald. LED based Spectroscopy – a Low Cost Solution for High Resolution Concentration Measurements e.g. for Gas Monitoring Applications. 2011. DOI:10.1109/ICSensT.2011.6136951.

[37] S. Landgraf. Use of Ultrabright LEDs for the Determination of Static and Time-Resolved Fluorescence Information of Liquid and Solid Crude Oil Samples. *Journal of Biochemical and Biophysical Methods*, 61:125–134, 2004. DOI:10.1016/j.jbbm.2004.04.003.

[38] APA102c RGB-LED datasheet. `https://cdn-shop.adafruit.com/datasheets/APA102.pdf`. Accessed 8.12.2017.

[39] 430 nm blue LED datasheet. `http://www.farnell.com/datasheets/55778.pdf`. Accessed 8.12.2017.

[40] Edmund Optics. Optics Application examples. `https://www.edmundoptics.es/resources/application-notes/optics/optics-application-examples/`. Accessed 8.12.2017.

[41] Edmund Optics. Comparison of Optical Aberrations. `https://www.edmundoptics.com/resources/application-notes/optics/comparison-of-optical-aberrations/`. Accessed 8.12.2017.

[42] B. Long. *Complete Digital Photography*. Charles River Media, 4 edition, 2007.

[43] FLIR Integrated Imaging Solutions, Inc. How to Evaluate Camera Sensitivity. `https://www.ptgrey.com/white-paper/id/10912`. Accessed 8.12.2017.

[44] P. Hiscocks. Measuring Luminance with a Digital Camera. 2014. Available on `https://www.ee.ryerson.ca/~phiscock/astronomy/light-pollution/luminance-notes-2.pdf`. Accessed 8.12.2017.

[45] Cambridge in Colour - a learning community for photographers. Digital Camera Sensors. http://www.cambridgeincolour.com/tutorials/camera-sensors.htm. Accessed 8.12.2017.

[46] Understanding Gamma Correction. http://www.cambridgeincolour.com/tutorials/gamma-correction.htm. Accessed 8.12.2017.

[47] Geant4 simulation toolkit webpage. http://geant4.cern.ch/. Accessed 8.12.2017.

[48] Full documentation for picamera module. https://picamera.readthedocs.io/en/release-1.13/index.html. Accessed 8.12.2017.

Appendix

Appendix has the Python2.7-codes that were used in this study. The first code includes the graphical user interface from which the settings can be adjusted and a measurement can be started. The second code is the analysis code for the pictures.

```
#!/usr/bin/python
# -*- coding: UTF-8 -*-

import os
import sys
import Tkinter as tk
import ttk
import time
import GaussianPlot as gp
import picamera
import smbus
import RPi.GPIO as GPIO

class LTMeasurement(tk.Frame):

    # Main program that includes all the buttons and widgets shown in the
        GUI
    def __init__(self, parent):
        tk.Frame.__init__(self)
        self.root = parent
        self.root.title("Liquid Transparacy Measurement")
        self.root.minsize(width=400, height=200)

        # LED configuration
        self.output_pin = 10
        GPIO.setmode(GPIO.BOARD)
        GPIO.setwarnings(False)
        GPIO.setup(output_pin, GPIO.OUT)

        # Entry for the sample the measurement is carried on with
        sample_lbl = tk.Label(root, text='What sample?')
        sample_lbl.grid(row=0, column=0, sticky=tk.W)
        self.sample = tk.StringVar()
        self.sample_entry = tk.Entry(root, textvariable=self.sample)
        self.sample_entry.insert(0, "??")
        self.sample_entry.grid(row=0, column=1, sticky=tk.W)

        # Buttons and entries for camera settings
        camera_lbl = tk.Label(root, fg="green", text="camera settings:")
        camera_lbl.grid(row=1, sticky=tk.W)
        time_lbl = tk.Label(root, text="exposure time: ")
        time_lbl.grid(row=2, column=0, sticky=tk.W)
```

```
42          self.expTime = tk.StringVar()
43          self.exp_entry = tk.Entry(root, textvariable=self.expTime)
44          self.exp_entry.insert(0, 150)
45          self.exp_entry.grid(row=2, column=1, sticky=tk.W)
46          second_lbl = tk.Label(root, text="micro seconds")
47          second_lbl.grid(row=2, column=1, sticky=tk.E)
48          iso_lbl = tk.Label(root, text="ISO value: ")
49          iso_lbl.grid(row=3, column=0, sticky=tk.W)
50          self.isoVal = tk.StringVar()
51          self.iso_entry = tk.Entry(root, textvariable=self.isoVal)
52          self.iso_entry.insert(0, 100)
53          self.iso_entry.grid(row=3, column=1, sticky=tk.W)
54
55          # Entry for number of pictures to be taken
56          pic_lbl = tk.Label(root, text="Picture number: ")
57          pic_lbl.grid(row=4, column=0, sticky=tk.W)
58          self.pic_number = tk.StringVar()
59          self.pic_entry = tk.Entry(root, textvariable=self.pic_number)
60          self.pic_entry.insert(0, 10)
61          self.pic_entry.grid(row=4, column=1, sticky=tk.W)
62
63          # LED on/off-button, start-button, and
64          # quit-button
65          self.led_btn = tk.Button(root, text="LED on",
66                                   command=self.led_on_off, bg="green")
67          self.led_btn.grid(row=5, column=0, sticky=tk.W)
68          start_btn = tk.Button(root, text="Start",
69                                command=self.measurement)
70          start_btn.grid(row=5, column=1, sticky=tk.W)
71          quit_btn = tk.Button(root, text="Quit",
72                               command=self.close_window)
73          quit_btn.grid(row=5, column=1, sticky=tk.E)
74
75          # Progress bar for measurement
76          self.progress_var = tk.DoubleVar()
77          self.progress = ttk.Progressbar(root, orient="horizontal",
78                                          length=300, mode="determinate",
79                                          variable=self.progress_var)
80          self.progress.grid(row=6, column=0, columnspan=2)
81
82      # Doing the measurement
83      def measurement(self):
84          dir_name = self.make_measurement_dir()
85          self.cam(dir_name)
86          data = gp.get_profile(dir_name + '/pictures/')
87          self.make_info(dir_name)
88
89      # Putting LED on and off
90      def led_on_off(self):
```

```
91          led_command = self.led_btn.cget("text")
92          if led_command == 'LED on':
93              GPIO.output(output_pin, True)
94              self.led_btn.config(text="LED off")
95              self.led_btn.config(bg="red")
96          if led_command == 'LED off':
97              GPIO.output(output_pin, False)
98              self.led_btn.config(text="LED on")
99              self.led_btn.config(bg="green")
100
101     # Taking a set number of pictures
102     def cam(self, dir_name):
103         camera = picamera.PiCamera()
104         camera.resolution = (1280, 720)
105         iso = int(self.isoVal.get())
106         camera.ISO = iso
107         camera.vflip = True
108         camera.hflip = True
109         camera.framerate = 1
110         camera.awb_mode = 'off'
111         camera.awb_gains = (0.9, 1.9)
112         speed = int(self.expTime.get())
113         camera.shutter_speed = int(speed)
114         time.sleep(2)
115         camera.exposure_mode = 'off'
116         EXPOSURE = camera.shutter_speed
117         SPEED = speed
118         pic_max = int(self.pic_number.get())
119         self.progress.config(maximum=pic_max-1)
120
121         i = 0
122         try:
123             while i < pic_max:
124                 self.progress_var.set(i)
125                 camera.capture(dir_name + '/pictures/pic%s' % (i + 1), '
                        jpeg')
126                 i += 1
127                 root.update_idletasks()
128             pass
129         finally:
130             camera.close()
131
132     # Make a directory for the measurement
133     def make_measurement_dir(self):
134         date = time.strftime("%Y-%m-%d")
135         DIR_NAME = '/home/pi/Desktop/measurements/'
136         nro = 1
137         while True:
138             dir_name = DIR_NAME + date + '_measurement_' + str(nro)
```

```
139             if not os.path.exists(dir_name):
140                 os.makedirs(dir_name + '/pictures/')
141                 break
142             else:
143                 nro += 1
144         return dir_name
145 
146     # Make info.txt for the measurement
147     def make_info(self, dir_name):
148         sample = self.sample.get()
149         led_color = self.c_box.get()
150         exposure = self.expTime.get()
151         iso = self.isoVal.get()
152         f = open(dir_name + '/info.txt', 'w')
153         f.write(time.strftime("%d/%m/%Y %H:%M:%S %Z\n"))
154         f.write('Sample: %s\n' % sample)
155         f.write('Given exposure speed: %s ms\n' % exposure)
156         f.write('ISO value: %s\n' % iso)
157         f.close()
158 
159     # Turn off the LED and the measurement window
160     def close_window(self):
161         GPIO.cleanup()
162         self.root.destroy()
163         sys.exit(0)
164 
165 if __name__ == "__main__":
166     root = tk.Tk()
167     app = LTMeasurement(root)
168     root.mainloop()
```

Separate Python code for the analysis part:

```
#!/usr/bin/python
# -*- coding: UTF-8 -*-

import os
import numpy as np
from PIL import Image
import cv2
import matplotlib.pyplot as plt
from matplotlib import cm
from scipy.optimize import curve_fit
import sys

# Define 2D Gaussian function
def gauss_2D((x, y), a, x0, y0, sigmax, sigmay, offset):
    f = offset + a*np.exp(-(x-x0)**2/(2*sigmax**2) - (y-y0)**2/(2*sigmay
        **2))
    return f.ravel()

# Get the list of images in the image directory
dir_name = {NAME OF THE MEASUREMENT DIRECTION} + '/pictures/'
images = os.listdir(dir_name)

# Number of images
n = len(images)

# Numpy-array for the average pixel values
size = 1800
arr = np.zeros((size, size), np.float)

# CALCULATING THE AVERAGE PIXEL ARRAY
# Getting the sum of every image array in a measurement
for img in images:
    im = cv2.imread(dir_name + str(img))
    gray = cv2.cvtColor(im, cv2.COLOR_BGR2GRAY)
    imarr = np.array(gray, dtype=np.float64)
    imarr = imarr[996 - size/2:996 + size/2, 1231 - size/2:1231 + size/2]
    arr = arr + imarr

# The mean of the image arrays
arr = arr/n

# CALCULATING ERROR FOR EVERY PIXEL VALUE
# Numpy-array for the errors
err = np.zeros((size, size), np.float)

for img in images:
    im = cv2.imread(dir_name + str(img))
```

```
47      gray = cv2.cvtColor(im, cv2.COLOR_BGR2GRAY)
48      imarr = np.array(gray, dtype=np.float64)
49      imarr = imarr[996 - size/2:996 + size/2, 1231 - size/2:1231 + size/2]
50      err = err + (imarr - arr)**2
51
52  err = np.sqrt(err/n)
53  err = err/np.sqrt(n)
54
55  # THE CODE BELOW FITS THE 2D GAUSSIAN TO THE DATA AND MAKES THE PLOT
56  x = np.linspace(0, size-1, size)
57  y = np.linspace(0, size-1, size)
58  x, y = np.meshgrid(x, y)
59
60  x_profile = arr[size/2,:]
61  y_profile = arr[:,size/2]
62
63  z = arr.ravel()
64  zerr = err.ravel()
65
66  # Initialization of the fit parameters
67  a = np.amax(z)
68  offset = np.amin(z)
69  x0 = size/2
70  y0 = x0
71  sigmax = np.std(x_profile, dtype=np.float64)
72  sigmay = np.std(y_profile, dtype=np.float64)
73
74  # Fitting 2D Gaussian to the data
75  popt, pcov = curve_fit(gauss_2D, (x, y), z, p0=[a, x0, y0, sigmax, sigmay
        , offset])
76  data_fitted = gauss_2D((x, y), *popt)
77  perr = np.sqrt(np.diag(pcov))
78
79  plt.style.use('ggplot')
80  fig, ax = plt.subplots(1, 1)
81  plt.contourf(z.reshape(size, size), 20, cmap=plt.cm.viridis, vmin=0, vmax
        =255)
82  plt.colorbar()
83
84  a = 'A=%s $\pm$ %s\n' % (round(popt[0], 3), round(perr[0], 3))
85  x0 = 'x$_0$=%s $\pm$ %s\n' % (round(popt[1], 3), round(perr[1], 3))
86  y0 = 'y$_0$=%s $\pm$ %s\n' % (round(popt[2], 3), round(perr[2], 3))
87  sigmax = '$\sigma_x$=%s $\pm$ %s\n' % (round(popt[3], 3), round(perr[3],
        3))
88  sigmay = '$\sigma_y$=%s $\pm$ %s\n' % (round(popt[4], 3), round(perr[4],
        3))
89  offset = 'offset=%s $\pm$ %s\n' % (round(popt[5], 3), round(perr[5], 3))
90
91  t = 'Fit parameters:\n' + a + x0 + y0 + sigmax + sigmay + offset
```

```
92 ax.annotate(t, xy=(0, 1), xytext=(15, -15), fontsize=10,
93              xycoords='axes fraction', textcoords='offset points',
94              bbox=dict(facecolor='white', alpha=0.8),
95              horizontalalignment='left', verticalalignment='top')
96 plt.title(sample + ' sample' + bubble)
97 plt.ylabel('Position y (pixel)')
98 plt.xlabel('Position x (pixel)')
99 plt.grid(False)
100 plt.show()
```